JCB Journal of Cell Biology

ARTICLE

$PI(4,5)P_2$ controls plasma membrane PI4P and PS levels via ORP5/8 recruitment to ER–PM contact sites

Mira Sohn[1], Marek Korzeniowski[1], James P. Zewe[2], Rachel C. Wills[2], Gerald R.V. Hammond[2], Jana Humpolickova[3], Lukas Vrzal[3], Dominika Chalupska[3], Vaclav Veverka[3], Gregory D. Fairn[4], Evzen Boura[3], and Tamas Balla[1]

Phosphatidylinositol 4,5-bisphosphate ($PI(4,5)P_2$) is a critically important regulatory lipid of the plasma membrane (PM); however, little is known about how cells regulate PM $PI(4,5)P_2$ levels. Here, we show that the phosphatidylinositol 4-phosphate (PI4P)/phosphatidylserine (PS) transfer activity of the endoplasmic reticulum (ER)–resident ORP5 and ORP8 is regulated by both PM PI4P and $PI(4,5)P_2$. Dynamic control of ORP5/8 recruitment to the PM occurs through interactions with the N-terminal Pleckstrin homology domains and adjacent basic residues of ORP5/8 with both PI4P and $PI(4,5)P_2$. Although ORP5 activity requires normal levels of these inositides, ORP8 is called on only when $PI(4,5)P_2$ levels are increased. Regulation of the ORP5/8 attachment to the PM by both phosphoinositides provides a powerful means to determine the relative flux of PI4P toward the ER for PS transport and Sac1-mediated dephosphorylation and PIP 5-kinase–mediated conversion to $PI(4,5)P_2$. Using this rheostat, cells can maintain $PI(4,5)P_2$ levels by adjusting the availability of PI4P in the PM.

Introduction

Despite their small amount, inositol phospholipids play critical roles in the organization of most cellular activities (Balla, 2013). Phosphatidylinositol 4,5-bisphosphate ($PI(4,5)P_2$), in particular, is one of the most important phosphoinositides found in the plasma membrane (PM), not only serving as precursor for both phospholipase C (PLC)–generated and phosphatidylinositol 3-kinase–generated messengers, but also directly regulating the activity of many integral membrane ion channels and transporters. $PI(4,5)P_2$ also contributes to membrane remodeling activities such as endo- and exocytosis (Balla, 2013). $PI(4,5)P_2$ is produced from PM phosphatidylinositol 4-phosphate (PI4P) by PIP 5-kinases, and therefore, the PI4P supply is critical for the maintenance of $PI(4,5)P_2$ in the PM. The major source of PM PI4P is PI4KA (Balla et al., 2008; Nakatsu et al., 2012; Bojjireddy et al., 2014), one of four distinct PI 4-kinase enzymes (Boura and Nencka, 2015), which is recruited to the PM by a protein complex formed by EFR3, TTC7, and Fam126 (Nakatsu et al., 2012; Baskin et al., 2016).

Although PM PI4P has long been known to serve as a precursor of $PI(4,5)P_2$, several recent observations suggest a more complex picture concerning the roles of PM PI4P. First, $PI(4,5)P_2$ levels can be maintained at various PI4P levels in the PM (Hammond et al., 2012, 2014; Nakatsu et al., 2012; Bojjireddy et al., 2014), and second, as long as PLC is not activated, pharmacological inhibition or genetic inactivation of PI4KA does not lead to significant $PI(4,5)P_2$ depletion, despite the reduction of PM PI4P to almost undetectable levels (Nakatsu et al., 2012; Bojjireddy et al., 2014; Hammond et al., 2014). Third, PM PI4P is transported back to the ER at ER–PM contact sites by the lipid transport proteins ORP5 and ORP8 to support the countertransport of phosphatidylserine (PS) by the same proteins (Chung et al., 2015). This lipid-exchange mechanism is conserved from yeast to humans (Maeda et al., 2013; Moser von Filseck et al., 2015). These findings raise the question of how cells control the fraction of PM PI4P to be converted to $PI(4,5)P_2$ relative to the amount that is transferred to the ER by the ORP proteins.

In the present study, we describe unique regulatory features of the ORP5 and ORP8 proteins. We show that the lipid transport activity of these proteins depends on the levels of both PI4P and $PI(4,5)P_2$ within the PM. Although ORP5 activity requires both of these inositides at their normal PM levels, ORP8 is called on only when $PI(4,5)P_2$ levels are increased. Such control provides an efficient way to adjust PI4P removal by the two ORPs according to the PM availability of PI4P and $PI(4,5)P_2$. This intricate regulatory mechanism ensures that the level of $PI(4,5)P_2$ is kept within a narrow range to fulfill its multiple cellular functions.

[1]Section on Molecular Signal Transduction, Eunice Kennedy Shriver National Institute of Child Health and Human Development, National Institutes of Health, Bethesda, MD; [2]Department of Cell Biology, University of Pittsburgh School of Medicine, Pittsburgh, PA; [3]Institute of Organic Chemistry and Biochemistry of the Czech Academy of Sciences, Prague, Czech Republic; [4]Keenan Research Centre for Biomedical Science, St. Michael's Hospital, Toronto, ON, Canada.

Correspondence to Tamas Balla: ballat@mail.nih.gov.

Supplemental material can be found at:
http://doi.org/10.1083/jcb.201710095

https://doi.org/10.1083/jcb.201710095

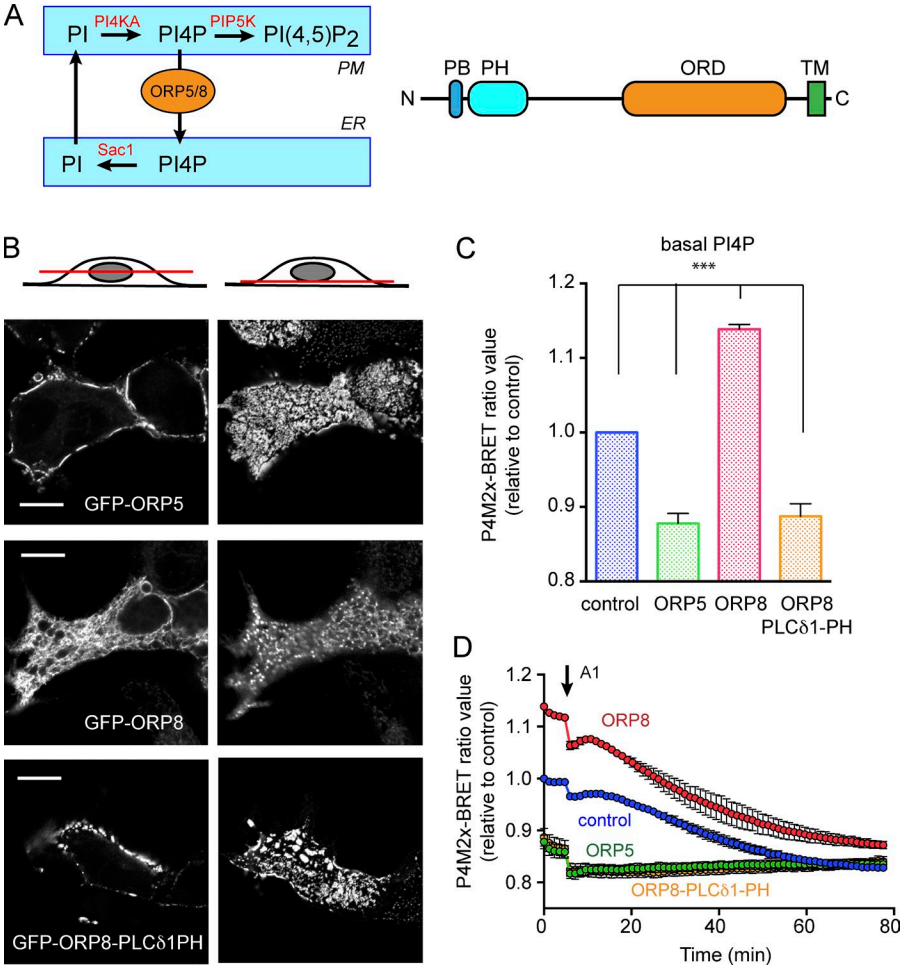

Figure 1. **PM interaction of ORP5/8 determines level of PI4P in the PM. (A)** PI4P metabolism at ER-PM contact sites (left) and a linear domain structure of ORP5/8 (right). After being synthesized by PI4KA, PI4P is either phosphorylated by PIP5K to $PI(4,5)P_2$ in the PM or transported to the ER. In the ER, PI4P is dephosphorylated by Sac1 phosphatase (left). Both ORP5 and ORP8 consist of a polybasic (PB) domain, a PH domain, an OSBP-related domain (ORD), and a transmembrane (TM) domain from N to C terminus (right). **(B)** Intracellular localization of ORP5, ORP8, and ORP8-PLCδ1-PH in live cells. HEK293-AT1 cells were transfected with GFP-tagged ORP5, ORP8, or ORP8-PLCδ1-PH and observed with confocal microscopy after 1 d. The same group of cells was observed on both the middle focal plane (left) and the bottom focal plane (right). Bars, 10 µm. **(C)** Quantitation of PM PI4P levels in live HEK293-AT1 cells with overexpression of ORP5, ORP8, or ORP8-PLCδ-PH by BRET analysis (see Materials and Methods for details). Grand means ± SEM are shown from three independent experiments performed in triplicate and normalized to the mean BRET value of mCherry-transfected (control) cells. Statistical significance was obtained with one-way ANOVA ($P < 0.005$). **(D)** Kinetics of PM-PI4P decrease by A1 treatment in BRET analysis. After measuring baseline BRET signal as shown in C, cells were treated with A1 (30 nM) and monitored for PI4P decrease. Grand means ± SEM are shown from three independent experiments performed in triplicate and normalized to the initial BRET value of mCherry-transfected (control) cells.

Results

ORP5/8 differentially regulate PM PI4P levels through different engagement with the PM

ORP5 and ORP8 are highly similar in their primary sequence. Both ORPs possess an N-terminal Pleckstrin homology (PH) domain followed by a lipid transfer domain, and a C-terminal transmembrane domain that anchors the proteins to the ER (Olkkonen and Li, 2013; Fig. 1 A). To compare the features of the two ORP proteins, we used N-terminally tagged GFP versions of either ORP5 or ORP8 expressed in HEK293 cells. Despite their structural similarities, we observed significant differences between the subcellular localizations of the two proteins. Although ORP5 was found tightly associated with the PM, ORP8 showed very poor PM interaction (Fig. 1 B). This difference in the intracellular localizations of ORP5 and ORP8 was already documented by Chung et al. (2015). The poor PM localization of ORP8 was clearly related to its PH domain because its replacement with the PH domain of PLCδ1, which strongly binds PM $PI(4,5)P_2$, turned ORP8 localization similar to that of ORP5 (Fig. 1 B). Despite showing similar localizations, ORP5 and ORP8-PLCδPH responded differently to PM PI4P depletion. Pharmacological inhibition of PI4KA by treatment with the specific inhibitor, A1, which depletes PI4P without affecting $PI(4,5)P_2$ levels in the PM (Bojjireddy et al., 2014), caused a slow ORP5 dissociation from the PM but did not affect the localization of ORP8-PLCδPH (Fig. S1 A, bottom). Only when PM $PI(4,5)P_2$ was also decreased after stimulation with the Gq-coupled angiotensin II (AngII) receptor did ORP8-PLCδPH disengage from the PM (Fig. S1 A).

To investigate the effects of the expression of ORP5, ORP8, and ORP8-PLCδPH on the dynamics of PI4P in the PM, we used the bioluminescence resonance energy transfer (BRET) method developed by the Varnai group (Tóth et al., 2016; Várnai et al., 2017; Fig. S1 B). BRET efficiency depends on the proximity between a membrane-anchored Venus protein and a Renilla luciferase–fused lipid-binding probe of our choice, in this case P4M(2x) (Hammond et al., 2014). The effect of ORP5 and -8 overexpression on PM PI4P levels was strikingly different: PI4P was dramatically reduced in ORP5-expressing cells, whereas it was significantly increased in ORP8-expressing cells compared with vector-transfected controls (Fig. 1 C). Although the increased PI4P levels after ORP8 overexpression was unexpected (see explanation in the Discussion), expression of ORP8-PLCδPH reduced PM PI4P to a level similar to ORP5 (Fig. 1 C). These results suggested that the differential engagement of ORP5 and ORP8 with the PM could be responsible for the opposite effects of the two proteins on PM PI4P levels.

PI4P transport correlates with the strength of ORP5/8 PM interaction

After synthesis by PI4KA, PM PI4P can be either converted to $PI(4,5)P_2$ or delivered to the ER by ORP5/8 proteins, where it is

dephosphorylated by the ER-resident phosphatase Sac1 (Fig. 1 A). (It should be noted that some studies suggested that Sac1 can act on PM PI4P acting in trans at ER–PM contact sites [Stefan et al., 2011; Dickson et al., 2016]). To address the question of how the PI4P clearance from the PM is affected by overexpression of ORP5, ORP8, or ORP8-PLCδPH, we measured the kinetics of PI4P decrease in the PM after treatment with the PI4KA inhibitor, A1 (Bojjireddy et al., 2014). As described previously (Sohn et al., 2016), PM PI4P levels declined steadily after A1 treatment in control HEK293 cells (Fig. 1 D, blue). The elevated level of PM PI4P in ORP8-expressing cells was associated with only a slightly accelerated clearance of PM PI4P after A1 treatment (Fig. 1 D, red). In contrast, after A1 treatment in ORP5-expressing cells, the substantially diminished levels in PM PI4P showed a very rapid drop to levels that we considered the detection limit of this method (Fig. 1 D, green). Expression of ORP8-PLCδPH had similar effects as ORP5 on both the basal PM PI4P basal levels and the rapid clearance from the PM (Fig. 1 D, orange). Although ORP8-PLCδPH was expected to work even when low PI4P levels would prevent ORP5 PM interaction, we could not detect a difference in PI4P levels, which may be related to the insensitivity of this method at the low end of PI4P levels.

Next, we investigated whether such changes in PM PI4P levels had any impact on $PI(4,5)P_2$ levels or their recovery after AngII stimulation. For this, we measured $PI(4,5)P_2$ changes in the PM using the PLCδ1 PH domain as a reporter in the BRET measurements. The basal level of $PI(4,5)P_2$ showed a small but consistent increase after expression of either ORP5 or ORP8. However, the resynthesis of PM $PI(4,5)P_2$ after AngII stimulation was impaired in cells expressing ORP5 compared with controls or cells expressing ORP8 (Fig. 2 A). This result was consistent with earlier conclusions (Bojjireddy et al., 2014) that maintenance of $PI(4,5)P_2$ levels during strong PLC activation is limited by the availability of PM PI4P.

The lipid transfer domains of both ORP5 and ORP8 can transfer PI4P from the PM

Our data suggested that the PI4P transfer activity of ORPs depended on their strong interaction with the PM, which, in turn, was determined by the PI4P content of the membrane. However, these results did not tell us about the relative abilities of these proteins to transport PI4P. To investigate this feature of the ORPs independently from the differences observed in the PM interactions of the two proteins, we replaced the PH domains in both ORP5 and ORP8 with an FK506-binding protein (FKBP12) module in an mCherry-tagged form (mCherry-FK-ORP5/8). This design allowed us to acutely switch on the PM interaction of the proteins with a PM-targeted FRB and the addition of rapamycin. Using this system, we monitored PI4P changes in the PM after recruitment of the FKBP-fused ORP5/8 proteins to the PM. As shown in Fig. 2 B, Recruitment of either FK-ORP5 or FK-ORP8 rapidly extracted PI4P from the PM, and FK-ORP8 showed even higher activity compared with FK-ORP5 in this assay (Fig. 2 B, red). Collectively, these data show that both proteins are able to extract PI4P from the PM and suggest that the differential activity of the full-length proteins is purely reflected in their different engagement with the PM.

Using the same assay, we also examined whether these ORPs could extract other lipids from the PM. These studies showed that ORP5 was able to extract PS, whereas ORP8 was able to do so only when competing PI4P levels were decreased in the PM, and even then, it was not very active (Fig. S2 A). Neither of these proteins extracted $PI(4,5)P_2$ or cholesterol from the PM as measured by this assay (Fig. S2, B and C)

Interaction of ORP5/8 with the PM requires both PI4P and $PI(4,5)P_2$

The ability of both ORP5 and ORP8 to efficiently extract PI4P from the PM prompted us to take a closer look at the factors that determine the membrane engagement of the two proteins. It has already been established that PI4P was required for PM interaction (Chung et al., 2015; Sohn et al., 2016). Yet the fact that these proteins showed no interaction with other PI4P-containing membranes, such as the Golgi, suggested that additional PM-specific components were required. To address the question of whether $PI(4,5)P_2$ might be one of these factors, we acutely reduced $PI(4,5)P_2$ in the PM, either alone or in combination with PI4P, using the recruitable pseudojanin (FKBP-PJ) enzyme (Hammond et al., 2012) and followed the interaction of ORP5 with the PM by total internal reflection fluorescence (TIRF) analysis. FKBP-PJ is a hybrid fusion protein built from the Sac1 (4-phosphatase) domain of the yeast Sac1 and the 5-phosphatase domain of human INPP5E. Inactivating mutations in either the Sac1 or the 5-phosphatase domains allows separate or combinational acute control of PI4P or $PI(4,5)P_2$ levels in the PM (Hammond et al., 2012). (It should be noted, however, that for acute $PI(4,5)P_2$ depletion, we used the more active single 5-phosphatase domain of INPP5E and not the FKBP-PJ 5-phosphatase active mutant enzyme in this study.) This analysis showed that acute reduction of either PI4P or $PI(4,5)P_2$, alone or in combination, effectively disengaged ORP5 from the PM in COS-7 cells (Fig. 2 C). Recruitment of a catalytically inactive FKBP-PJ (PJ-dead) did not change the interaction of ORP5 with the PM (Fig. 2 C). Similar experiments performed in HEK293 cells and analyzed by confocal microscopy also showed the striking localization change of ORP5 under the depletion of PM $PI(4,5)P_2$ using the recruitable INPP5E 5-phosphatase domain (Varnai et al., 2006; Fig. S3 A).

The finding that ORP8 showed substantially fewer and smaller contacts with the PM raised the question of whether this protein would require increased PM $PI(4,5)P_2$ for proper PM interaction. To test this, we overexpressed an mRFP-tagged PIP 5-kinase construct consisting of a truncated form of mouse PIP5K1β (human nomenclature) and monitored GFP-ORP8 distribution by confocal microscopy. Strikingly, cells that expressed mRFP-PIP5Kβ showed prominent enrichment of ORP8 at the PM contrasting the mostly ER distribution of the protein in cells lacking mRFP-PIP5Kβ expression (Fig. 3 A). Expression of a kinase-inactive version of PIP5Kβ had a small effect, but in most cells that expressed mRFP-PIP5K-dead, ORP8 still showed primarily ER distribution (Fig. 3 A). (The small effect of the kinase-dead enzyme was attributed to its known dimerization [Lacalle et al., 2015] with endogenous PIP5K, which would bring some of the endogenous active kinase to the sites where the expressed enzyme is localized [mostly the PM].) Importantly, PI4P was still needed for ORP8

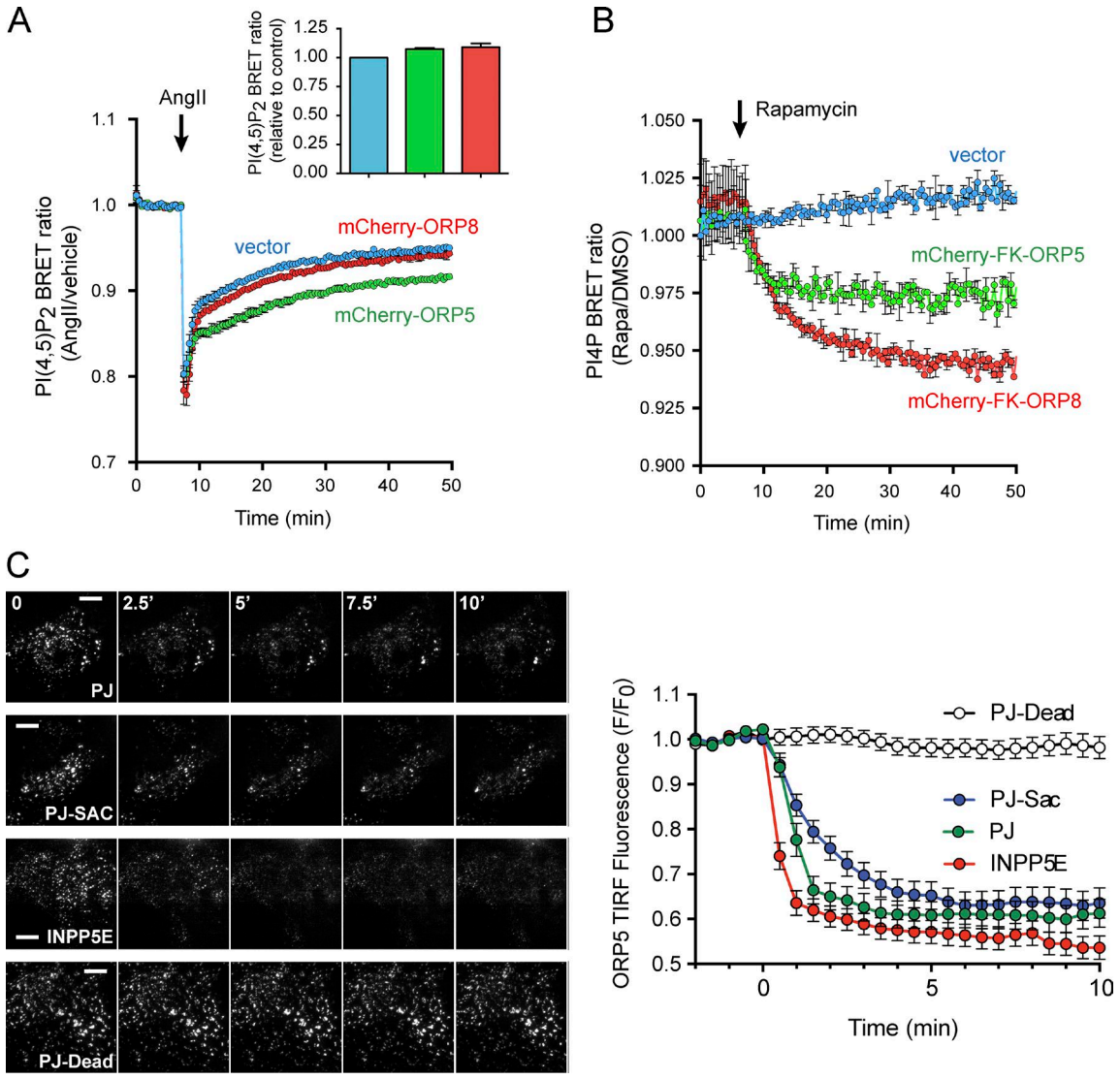

Figure 2. **PM binding of ORP5 depends on both PI4P and PI(4,5)P_2. (A)** Kinetics of PI(4,5)P_2 resynthesis after AngII stimulation in ORP5- or ORP8-expressing cells. HEK293-AT1 cells transfected with mCherry-tagged ORP5, ORP8, or mCherry were analyzed with BRET using PM-anchored Venus and PLCδ-PH–fused luciferase. After baseline measurement, cells were treated with vehicle or AngII (100 nM). Relative change in PI(4,5)P_2 level by AngII (AngII/vehicle) was normalized to the mean values gained from baseline measurements (the baseline values showed a slight increase both with ORP5 and ORP8 expression as shown in the insert). Grand means ± SEM are shown from three independent experiments performed in triplicate. **(B)** Quantitation of PI4P changes after PM recruitment of FKBP12-fused ORP5/8. HEK293-AT1 cells were transfected with mCherry or mCherry-tagged FKBP-ORP5 (FK-ORP5) or -ORP8 (FK-ORP8) in addition to PM-anchored FRB (PM2-FRB). PM PI4P levels were quantitated with BRET analysis using PM-anchored Venus and P4M(2x)-fused luciferase. After baseline measurement, cells were treated with DMSO or rapamycin (100 nM) for recruiting FK-ORP5 or -ORP8 to the PM. Relative PI4P level (rapamycin/DMSO) was normalized to mean value of baseline measurement. Grand means ± SEM are shown from three independent experiments performed in triplicate. **(C)** ORP5-PM contacts in PM PI4P- or PI(4,5)P_2-depleted cells. COS-7 cells were transfected with GFP-tagged ORP5 and mCherry-tagged FKBP-PJ, -PJ-Sac, -PJ-Dead, or FKBP-INPP5E. Lyn_{11}-FRB-iRFP was transfected as a recruiter. 1 d after transfection, cells were imaged by time-lapse TIRF microscopy, inducing acute depletion of PI4P, PI(4,5)P_2, or both with the addition of 1 µM rapamycin at time 0. Representative images from the time-lapse 0, 2.5, 5, 7.5, and 10 min of rapamycin treatment (left). The graph shows normalized GFP-ORP5 fluorescence intensity in the evanescent field for 28–34 cells imaged across three independent experiments (means ± SEM). Bars, 10 µm.

membrane localization even when PI(4,5)P_2 production was increased, as treatment of the cells with A1 slowly abolished the PM localization of ORP8 (Fig. S3 C).

The N-terminal basic segment together with the PH domain are responsible for the different PI-binding behaviors of ORP5 and ORP8

Previous studies showed that the PH domains of ORP5/8 were responsible for PI4P binding and PM localization of the two proteins (Chung et al., 2015). We noted that the constructs used in that study included a polybasic segment that precedes the strictly defined PH domain (Fig. 3 B). When we compared the PM localization of the isolated PH domain of the ORP5/8 proteins with those also containing the adjacent polybasic segments (termed extended PH domain [ePH]), we found that the ePH probes showed stronger localization than the simple PH domains (Fig. 3 C). In either case, as also observed in Chung et al. (2015), the PM localizations of the ORP5-derived domains were stronger than those derived from

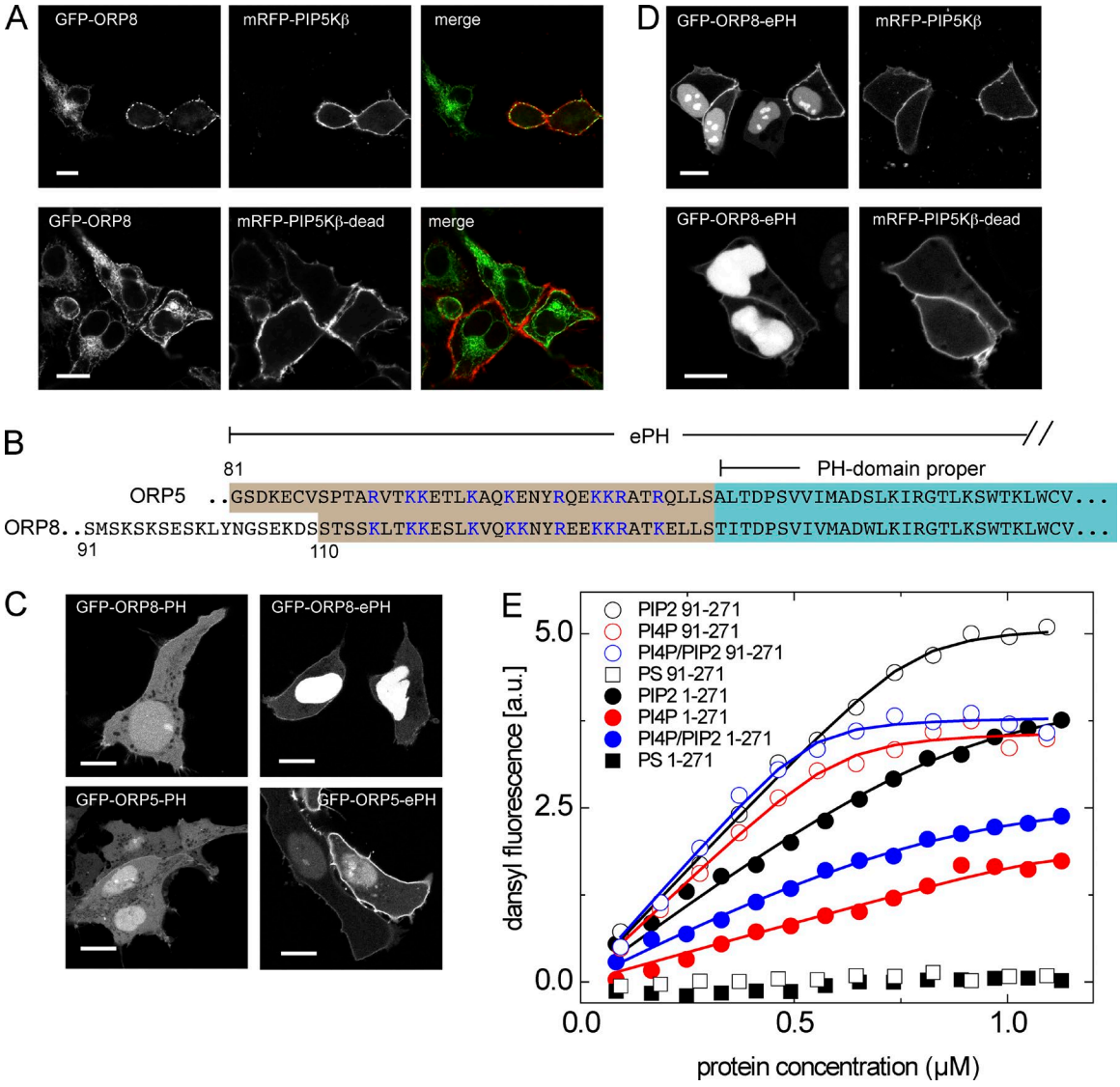

Figure 3. **Extra PI(4,5)P_2 production increases the PM engagement of ORP8. (A)** Representative live cell images showing intracellular localization of ORP8 under overexpression of PIP5Kβ. HEK293-AT1 cells were cotransfected with GFP-tagged ORP5 and wild-type or kinase-dead (dead) mRFP-tagged PIP5Kβ. After 1 d of transfection, cells were observed with confocal microscopy. Bars, 10 µm. **(B)** Comparison of amino acid sequences of N-terminal PH domains between ORP5 and ORP8. ORP5 and ORP8 share strictly defined PH domains (blue box). Conserved polybasic residues (blue) precede strict PH domains in both ORP proteins. **(C)** Representative live cell images showing localization of PH domains with or without adjacent polybasic residues. HEK293-AT1 cells were transfected with GFP-tagged ORP8-PH, ORP8-ePH, ORP5-PH, or ORP5-ePH. After 1 d, localization of PH domains was observed with confocal microscopy. Bars, 10 µm. **(D)** Representative live-cell images displaying effect of PIP5K overexpression in PM engagement of ORP8-ePH. HEK293-AT1 cells were cotransfected with GFP-tagged ORP8-ePH and mRFP-tagged PIP5Kβ (wild-type or kinase-dead). After 1 d, cells were observed with confocal microscopy. Bars, 10 µm. **(E)** Dependence of the Förster resonance energy transfer of ORP8 PH domain tryptophan residues to dansyl-labeled liposomes (monitored by dansyl fluorescence intensity) on the concentration of the PH domains. Solid and open circles, 1–284 and 91–284 constructs of the ORP8 PH domain. Liposomes contained 5 mol % of PI(4,5)P_2 (black), 5 mol % of PI4P (red), or 2.5 mol % of PI4P plus 2.5 mol % of PI(4,5)P_2 (blue). Squares, control liposomes bearing the same net charge from the negatively charged PS but no phosphoinositides. One representative result is shown from three separate experiments that gave identical results but differed in absolute fluorescent intensity values.

ORP8. Importantly, the PM localization of the ORP5-ePH showed the same dual requirement for PI4P and PI(4,5)P_2 binding as the full-length protein (Fig. S3 B). The strict PH domain of ORP8 barely localized to the PM, and even the ePH of ORP8 showed poor PM localization (Fig. 3 C). Importantly, PM localization of GFP-ORP8ePH was dramatically increased in the cells expressing mRFP-PIP5Kβ, but not its kinase-dead version (Fig. 3 D).

The dual PI-binding requirement for the localization of the N-terminal domains of ORP8 was further studied using recombinant proteins and in vitro liposome binding assays. For this, two constructs were expressed in bacteria, one containing ORP8 residues 91–284 (which is 18 residues longer toward the N terminus than ePH, which was necessary to obtain a stable protein) and another 1–284, which included the whole N terminus. It is noteworthy that the N terminus of ORP8 contains several acidic residues instead of the cluster of basic arginines found in ORP5. Liposomes containing the indicated phosphoinositides (5 mol % in total) were titrated by the two proteins, and the energy

transfer from tryptophan residues to dansyl-labeled liposomes was monitored (Fig. 3 E). Both constructs interacted with liposomes containing either PI4P or $PI(4,5)P_2$, and somewhat better binding was observed for $PI(4,5)P_2$-containing liposomes. The interaction was not a simple charge effect, because no binding to PS-containing liposomes was observed (Fig. 3 E, squares). Importantly, total PIP concentrations were the same for all the measurements (i.e., 5 mol %). Also, the overall charge, which was relatively high (assumed to correspond to 25 mol % PS), was kept the same by varying the concentration of the negatively charged PS lipid, and $PI(4,5)P_2$ was assumed to have the same charge as two molecules of PI4P. Notably, the longer construct showed reduced binding to all PIP-containing liposomes. This was consistent with the inhibitory nature of the more acidic N terminus of ORP8 observed by Chung et al. (2015); see also results shown in Fig. 7).

The ORP8 PH domain can bind either PI4P or $PI(4,5)P_2$

To understand the mode of PI recognition by ORP5/8 at the atomic level, we took advantage of the existing structure of ORP8 PH domain (PDB ID 1V88) that features the canonical PH domain fold with six β-sheets (β1–β6) packed against a single α-helix (Fig. 4 D). We followed changes in the backbone amide signals using NMR spectroscopy upon addition of PI4P or $PI(4,5)P_2$ ligands to reveal residues involved in phosphoinositide recognition. Several surface-exposed residues (Arg^{158}, Gly^{159}, Trp^{164}, Arg^{201}, Ser^{203}, Phe^{208}, Phe^{210}, Lys^{211}, Ile^{244}, and Arg^{246}) exhibited either signal intensity reduction or a significant change in the NMR signal position upon addition of the soluble PI4P or $PI(4,5)P_2$ analogues (Figs. 4 A and S4, A and B). The effects on NMR signal intensity or position for the entire PH domain are summarized in the graphs presented within Fig. 4 (B and C). When we identified the PI-responsive residues in the 3D structure of the ORP PH domain, we noted that they form a single patch that is larger in the case of $PI(4,5)P_2$ (Fig. 4 D, PI4P binding site in blue, $PI(4,5)P_2$ binding site in red). Notably, the PI4P and $PI(4,5)P_2$ binding sites we identified do overlap.

To obtain an atomistic model of PIP recognition by the ORP8 PH domain, we performed molecular dynamics simulation–assisted docking using the NMR data as restrains. This experiment revealed the putative binding mode used for PI4P and $PI(4,5)P_2$. Overall, the phosphate groups of both PIPs are recognized by arginine and lysine residues; whereas PI4P is held in place by 12 hydrogen bonds, $PI(4,5)P_2$ forms 16 hydrogen bonds, thereby explaining the higher affinity of ORP8 PH domain toward $PI(4,5)P_2$-containing liposomes. It should be noted that the polybasic stretch preceding the PH domain sequence was not resolved in the NMR structure, but it makes an important contribution to membrane binding based on our cellular studies.

PI4P transport from the PM to the ER is controlled by PM $PI(4,5)P_2$ levels

If PM $PI(4,5)P_2$ levels determine ORP5/8 localization, then we expected that PI4P transfer to be reduced when $PI(4,5)P_2$ levels are low. To test this, the rate of PI4P clearance from the PM was monitored under acute depletion of $PI(4,5)P_2$. Upon PM recruitment of the single 5-ptase domain of INPP5E, PM levels of $PI(4,5)P_2$ rapidly decreased as shown by BRET analysis (Fig. 5 A). Under the same conditions, the increase of PM PI4P was relatively small (Fig. 5 B). Addition of A1 to inhibit PI4KA at this point initiated the clearance of PI4P from the PM, which was significantly slower within cells in which $PI(4,5)P_2$ levels were reduced (Fig. 5 B). These results suggest that PI4P clearance by ORPs via transfer to the ER was reduced at low PM $PI(4,5)P_2$ levels.

We then attempted to perform the reverse experiment to test the effects of acute $PI(4,5)P_2$ increase on PM PI4P clearance by overexpression of a recruitable FKBP-PIP5Kγ. However, we found that overexpression of FK-PIP5Kγ, despite appearing to be exclusively cytosolic, for 1 d already significantly decreased the basal PI4P even without recruitment to the PM (Fig. S5 A). This finding suggests that prolonged expression of PIP5K results in a PI4P level reduction that becomes a limiting factor in PI4P transfer. To investigate this further, we performed a dose-dependent overexpression of myc-tagged full-length PIP5Kβ and tested the rate of PI4P elimination from the PM after A1 treatment. We found that the basal level of PI4P in the PM showed a dose-dependent decrease in response to overexpression of myc-PIP5Kβ (Fig. 5 C). The decrease in PM PI4P after overexpression of PIP5K was also demonstrated in confocal microscopy using the tandem GFP-P4M(2x) reporter as a probe to detect PI4P. Here, the PI4P reporter clearly relocalizes from the PM to the PI4P-rich endosomal and Golgi compartments specifically within the cells that express PIP5K (Fig. S5 B). Strikingly, cells transfected with a high amount of PIP5K not only had a low PM PI4P level, but also they showed only a very slow rate of PI4P clearance from the PM after inhibition of PI4KA with A1 (Fig. 5 C). Importantly, the decrease in the rate of PI4P clearance after A1 treatment shows good correlation with the drop observed in the initial PM PI4P levels determined using BRET measurements (Fig. 5 D). These observations suggest that prolonged activation of PIP5K leads to a decrease in PM PI4P levels and dissipation of the PI4P gradient to the point that it becomes limiting in PI4P transport from the PM.

PIP5K activity controls PM PI4P levels to limit substrate availability

The substantial decrease in PM PI4P levels in PIP5Kβ-expressing cells prompted us to investigate how the change in the levels of PI4P and $PI(4,5)P_2$ in these cells responds to AngII stimulation. As shown in Fig. 5 E, PI4P levels in the PM were greatly reduced in cells expressing PIP5Kβ, and the recovery after AngII stimulation was greatly impaired compared with control cells. In the case of $PI(4,5)P_2$, the basal levels were increased only slightly, and the recovery after stimulation was also impaired in spite of the presence of PIP5Kβ (Fig. 5 F). These data suggest that the PI4P decrease becomes limiting during resynthesis of $PI(4,5)P_2$ after PLC activation. These surprising data demonstrate that $PI(4,5)P_2$ levels are tightly controlled by altering PI4P availability through PI4P transport toward dephosphorylation within the ER.

ORP5/8 is important in the control of PI4P and $PI(4,5)P_2$ levels and their response to PIP5-kinase overexpression

To investigate the extent to which ORP5/8 plays a role in the control of resting PI4P and $PI(4,5)P_2$ levels as well as its role in the PI4P decrease observed after PIP5K overexpression, we performed experiments in cells with knockdown of ORP5/8 with

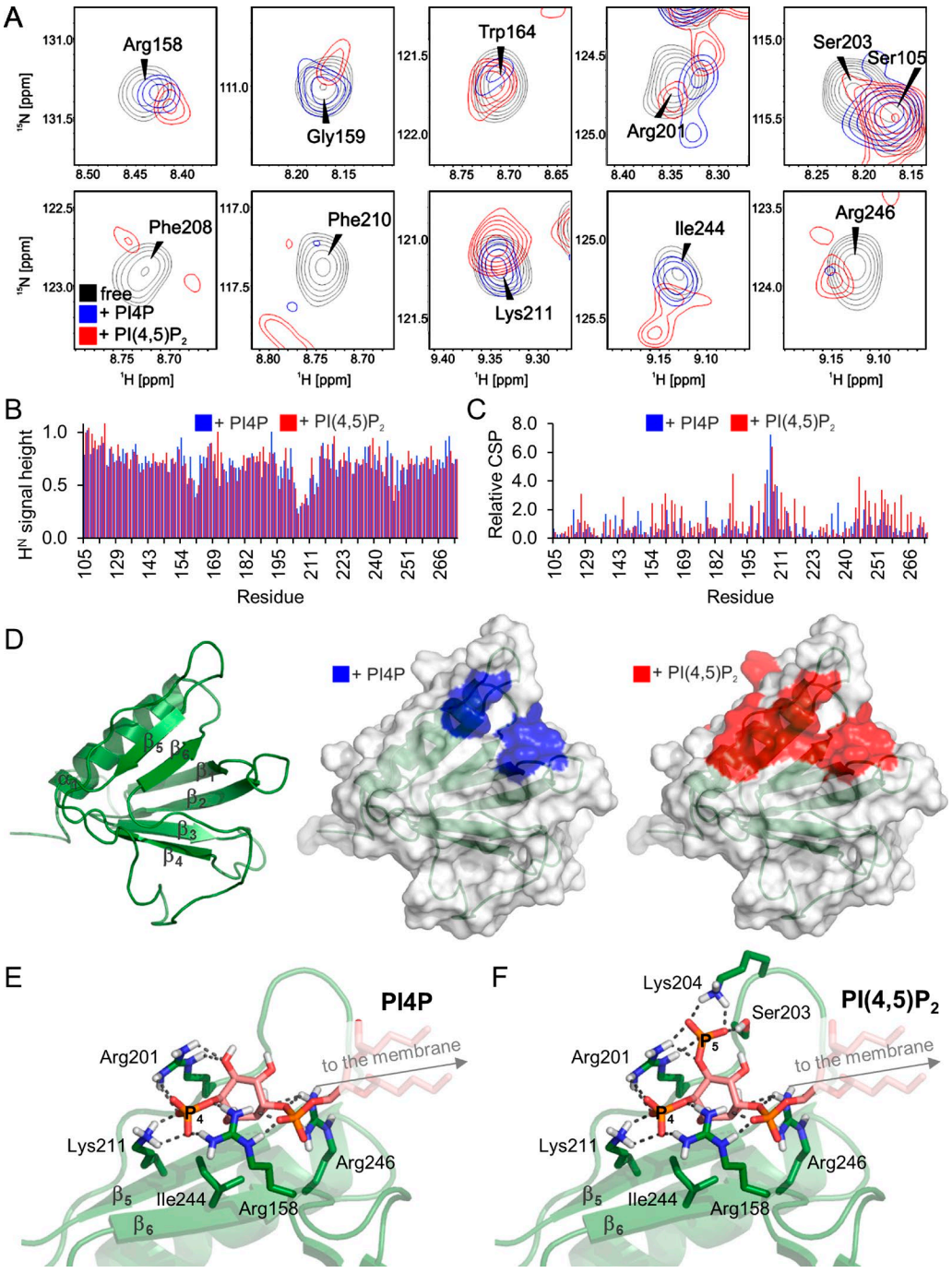

Figure 4. **Both PI4P and PI(4,5)P_2 bind to the PH domain of ORP8. (A)** The interaction with PI4P/PI(4,5)P_2 induced specific changes in the NMR spectra of ORP8. **(B and C)** We observed both significant reduction of signal intensity (B) and changes in positions of signals (C) in the 2D ^{15}N/^{1}H HSQC spectra of ^{15}N-labeled ORP8 PH domain upon the addition of the ligand. The graphs represent simple differences in signal positions and intensities between the free and ligand-bound protein obtained from a single experiment. **(D)** The PH domain adopts the canonical fold, and both PI4P and PI(4,5)P_2 bind to the same interface as suggested by highlighting the relative changes observed in the NMR spectra on the 3D protein structure. **(E and F)** The NMR-data driven models of the PH/PI4P (E) and PH/PI(4,5)P_2 (F) complexes suggest that the phosphate groups of PI4P/PI(4,5)P_2 are stabilized by an extensive network of electrostatic interactions with the positively charged side chains of Arg^{158}, Arg^{201}, Lys^{211}, and Arg^{246}. PI(4,5)P_2 is additionally stabilized by an interaction with Lys^{204} and Ser^{203}.

RNAi treatment (Fig. S5 C). As shown in Fig. 6 (A and B), combined ORP5 and ORP8 knockdown cells showed increased levels of both PI4P and PI(4,5)P_2, although the effects of the depletion of individual ORPs were variable. Importantly, the reducing effect of PIP5K overexpression on PI4P levels was significantly mitigated, although not completely reversed, by the combined knockdown of ORP5/8 (Fig. 6 C). This was confirmed also by confocal microscopy (Fig. 6 D). Combined knockdown of ORP5/8 consistently slowed down the rate of PI4P clearance after blocking PI4P production by A1 treatment, although this effect did not reach statistical significance. Moreover, the rate decrease caused by PIP5K overexpression was augmented rather than reversed

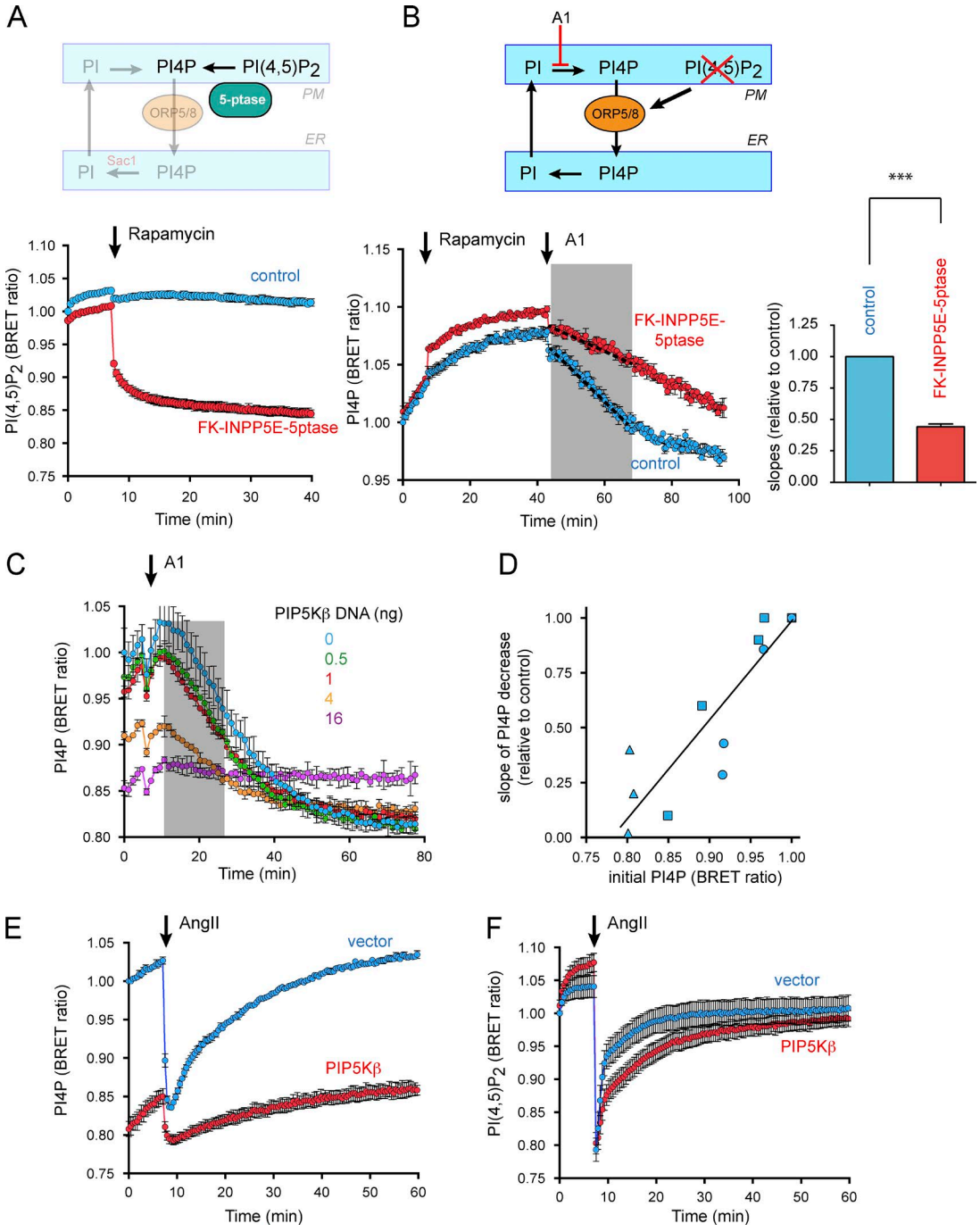

Figure 5. **PI4P transport is controlled by PI(4,5)P_2 levels in the PM. (A)** Acute depletion of PM PI(4,5)P_2 achieved by PM recruitment of INPP5E. The cartoon illustrates that PM-recruited 5ptase catalyzes dephosphorylation of PI(4,5)P_2 to PI4P in the PM (top). Changes in PM PI(4,5)P_2 levels were quantitated by BRET analysis before and after recruitment of 5ptase (bottom). HEK293-AT1 cells were cotransfected with mCherry-tagged FK-INPP5E and PM2-FRB before BRET analysis. Control cells were transfected with FK-PJ-dead plasmid instead of FK-INPP5E construct. After baseline measurement, cells were treated with DMSO or rapamycin for recruiting INPP5E to the PM. Relative PI(4,5)P_2 levels were normalized to the initial BRET value of control cells. Grand means ± SEM are shown from three independent experiments performed in triplicate. **(B)** Rate of PI4P clearance controlled by PM PI(4,5)P_2 levels. The cartoon illustrates that PM PI4P clearance after A1 treatment decreases when the ORP5/8-mediated transport is switched off as the 5ptase is recruited to the PM (top). PM PI4P clearance (after A1 addition) was monitored with or without PM PI(4,5)P_2 depletion in BRET analysis (bottom). HEK293-AT1 cells were cotransfected with PM2-FRB and FK-INPP5E together with the BRET construct before BRET measurement. Control cells were transfected with FK-PJ-dead instead of FK-INPP5E. After baseline measurement, cells were treated with rapamycin for recruiting FK-PJ-dead (control) or -INPP5E to the PM and subsequently with A1 (30 nM) as indicated by the arrows. Grand means ± SEM are shown from three independent experiments performed in triplicate and normalized to the initial BRET value of control cells. The gray area shows the time period for which the rate of decline was calculated in each experiment. These rate values are shown in the column diagram relative to the rates calculated in the controls (***, $P < 0.005$; $n = 3$). **(C)** Representative BRET experiment showing rate of PI4P clearance from the PM under dose-dependent overexpression of myc-tagged PIP5Kβ. HEK293-AT1 cells were transfected with 0 ng (blue), 0.5 ng (green), 1 ng (red), 4 ng (orange), and

by ORP5/8 knockdown. This finding indicates that ORP5/8 is important in redirecting PI4P toward Sac1-mediated degradation in response to PIP5K expression.

ORP8 exerts an inhibitory effect on ORP5 via its acidic N terminus

Because ORP5 and ORP8 has been shown to dimerize (Chung et al., 2015), we wanted to determine whether ORP5 could help ORP8 membrane association. Coexpression of the two proteins, however, revealed an opposite effect: ORP8 greatly reduced the association of ORP5 with the PM (Fig. 7 A). To investigate which part of ORP8 was responsible for this inhibitory effect, we generated truncated forms of ORP8. An ORP8 construct in which the PH domain was replaced with an FKBP module showed a reduced effect on ORP5 localization (Fig. 7 B). Similarly, an N-terminally truncated form of ORP8 in which the acidic first 100 residues were removed showed a reduced effect on ORP5 PM localization. In fact, in the latter case, ORP8 showed PM interaction and colocalization with ORP5 in punctate contact sites (Fig. 7 C). These results suggest that the acidic N terminus of ORP8 plays an important role in reducing the association of the two proteins with the PM.

PIP5K activity also controls PS distribution

Having seen the profound effect of PIP5K overexpression on PI4P levels and transport, it was an important question to address what happens to PS distribution in cells that overproduce PI(4,5)P_2. For this, we examined the localization of the PS reporter, Lact-C2 (Yeung et al., 2008) in cells overexpressing PIP5Kβ. Lact-C2 is normally found primarily in the PM with some signal associated with endosomes (see Sohn et al. [2016] for distribution in our HEK293 cells). Strikingly, this characteristic PS distribution was clearly altered in cells overexpressing PIP5Kβ, but less so when using a kinase-dead version of the protein (Fig. 8, A and B). Overall, the PM labeling by Lact-C2 was greatly reduced and was coupled with a clear increase in the endosomal localization, presumably because of the increased availability of the probe throughout the cytoplasm. These changes were also assessed by BRET using Lact-C2 as the lipid-binding domain within the BRET construct (Fig. S1 B, cartoon). This BRET analysis is in direct agreement with our confocal data, confirming that PIP5Kβ overexpression significantly reduces the level of PM PS and that the effect is much smaller in the presence of a kinase-dead version of PIP5Kβ (Fig. 8 C). The dynamic range of these measurements is shown in Fig. 8 D. Because PM PS can be rapidly eliminated from the inner leaflet of the PM by externalization, which can be acutely triggered by the large cytoplasmic Ca^{2+} increases, we used treatment with the Ca^{2+} ionophore, ionomycin, to determine the effective range for BRET measurements of PS. These limits were used to scale the plot shown in Fig. 8 C.

Discussion

This study was designed to better understand the mode of action and functional differences between the two lipid transfer proteins, ORP5 and ORP8. These two proteins are homologous and have been shown to function as PI4P/PS exchangers using PI4P gradients between the PM and the ER to transport PS from the ER and the PM (Chung et al., 2015). This lipid exchange mechanism has also been shown to function in yeast mediated by the Osh6 protein (Maeda et al., 2013; Moser von Filseck et al., 2015). Our experiments revealed that PM association of ORP5 and ORP8 relies on binding to both PI4P and PI(4,5)P_2, but there are major differences between the two proteins in their sensitivities to each phosphoinositide. Although the PM binding of ORP5 is fully supported by the resting levels of both PI4P and PI(4,5)P_2, the interaction of ORP8 is very poor under these conditions, but dramatically increases upon production of excess PI(4,5)P_2 in the PM. These features have a major impact on the control of PI4P transfer from the PM to the ER: a decrease in the level of either PI4P or PI(4,5)P_2 will reduce the transfer activity of ORP5 and ORP8, although ORP8 already makes little contribution under resting conditions. However, ORP8 becomes increasingly relevant upon stimulated production of PI(4,5)P_2, and even small increases in PI(4,5)P_2 profoundly enhance the association of ORP8 with the PM. This would enhance PI4P transfer from the PM to the ER but eventually dissipate the PI4P gradient between the two membranes, yielding a new steady state where PI4P levels are significantly decreased, thereby limiting both the PI4P transfer process and preventing the increases in PM PI(4,5)P_2 that could result from ample substrate availability combined with high activity of PIP5K.

This organization has the hallmarks of a rheostat mechanism aimed at keeping PM PI(4,5)P_2 levels within a narrow range. The ability of the ORP5/8 proteins to sense the total levels of PI4P and PI(4,5)P_2 and control PM PI4P levels via transport to the ER is uniquely suited to dynamically regulate PM PI(4,5)P_2. It is also worth pointing out that during strong PLC activation when both PI4P and PI(4,5)P_2 are decreased, PI4P transfer to the ER is substantially limited, not only via disengagement of ORP5/8 but also

16 ng (purple) DNA per well of myc-PIP5Kβ before BRET analysis. Means ± SD are shown from triplicate experments, normalized to the initial BRET value of the cells with no myc-PIP5Kβ (blue). **(D)** Rate of PI4P clearance correlated with initial PM PI4P levels (square symbols). Two more BRET experiments were conducted by transfecting 0, 2, 6, and 12 ng PIP5Kβ DNA per well (circles) or 0, 4, 8, and 16 ng of the myc-PIP5Kβ DNA per well (triangles), also performed in triplicate. After treatment of A1, PI4P reduction rate (slope designated in *y*-axis) was calculated from the highest levels (initial PI4P designated in *x*-axis) for 1,000-s. Relative reduction rates were normalized to initial PI4P levels with no myc-PIP5Kβ in each experiment. **(E)** Effect of PIP5Kβ overexpression on PM PI4P levels responding to AngII stimulation. HEK293-AT1 cells were transfected with pcDNA3.1(HA) vector or myc-tagged PIP5Kβ. Change in PM PI4P levels was analyzed with BRET. After baseline measurement, cells were simulated with AngII (100 nM). Grand means ± SEM are shown from three independent experiments performed in triplicate and normalized to the initial BRET value of vector-transfected cells. **(F)** Effect of PIP5Kβ overexpression in PM PI(4,5)P_2 levels responding to AngII stimulation. BRET analysis was conducted as described in E except that PM PI(4,5)P_2 levels were monitored. Grand means ± SEM are shown from three independent experiments performed in triplicate and normalized to the initial BRET value of vector-transfected cells.

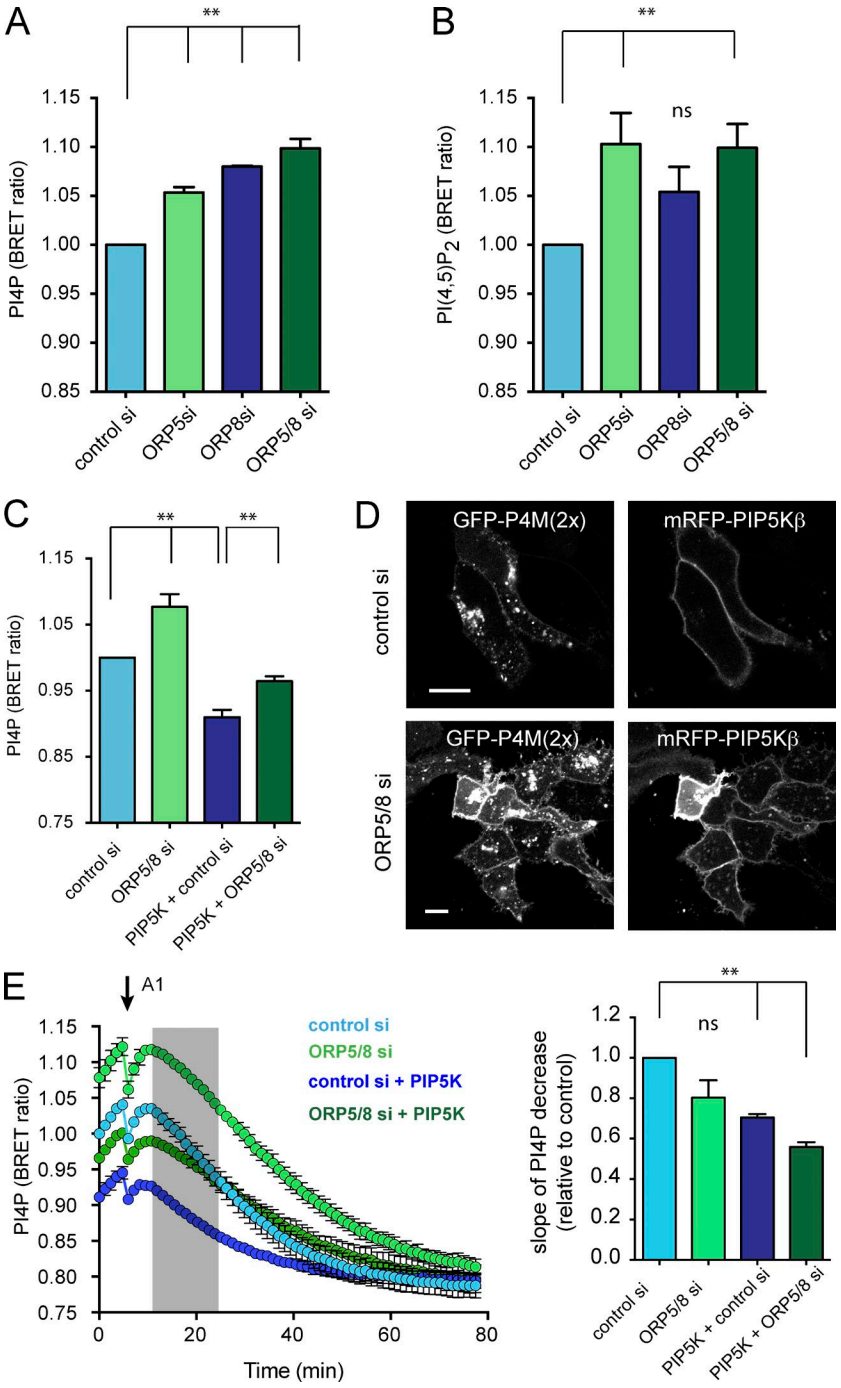

Figure 6. **Loss of ORP5/8 increases both PI4P and PI(4,5)P_2 levels in the PM. (A)** PM PI4P levels in ORP5-, ORP8-, or ORP5/8-depleted cells. HEK293-AT1 cells were transfected with control, ORP5-, ORP8-, or both ORP5- and ORP8-silencing siRNAs for 2 d and subjected to BRET analysis monitoring PM PI4P. Three independent experiments performed in triplicate were each normalized to control. Grand means ± SEM are shown. Statistical analysis was performed by two-way ANOVA (**, $P < 0.005$; ns, not significant). **(B)** Same experiments as in A except that PM PI(4,5)P_2 levels were assessed by BRET measurements. **(C)** Effect of knockdown of ORP5/8 on PI4P levels in PIP5Kβ-expressing cells. HEK293-AT1 cells were transfected with the indicated siRNAs as in A. 1 d after siRNA transfection, cells were transfected with pcDNA3.1(HA) or myc-tagged PIP5Kβ (2 ng/well). 1 d after DNA transfection, cells were subjected to BRET measurement for PM PI4P. Statistical analysis from three independent experiments performed in triplicate was obtained as described for A. **(D)** Representative live-cell confocal images showing changes in PI4P distribution in response to PIP5Kβ expression in cells treated with control or ORP5/8-targeting siRNAs. HEK293-AT1 cells were transfected with indicated siRNAs. 1 d after siRNA transfection, cells were cotransfected with GFP-tagged P4M(2x) and mRFP-tagged PIP5Kβ (50 ng/well). 1 d after DNA transfection, cells were observed with a confocal microscope. Note the presence of some PI4P in the PM even in the PIP5K-expressing cells in the ORP5/8-depleted cells. Bars, 10 µm. **(E)** Kinetics of PM PI4P decrease after A1 treatment (left) in cells expressing PIP5Kβ with or without depletion of ORP5/8. Experiment was as described in C except for treatment of cells with A1 (30 nM) after a control measurement period. The rate of PM PI4P decrease was calculated for the time period indicated by the gray area (D). Grand means ± SEM are shown from three independent experiments performed in triplicate. Values were normalized to the rate value calculated for the vector-transfected cells treated with control siRNA. Statistical analysis was obtained with two-way ANOVA (**, $P < 0.005$).

because of the disruption of PM–ER contacts (Giordano et al., 2013). Although this arrangement appears to be primarily useful for PI4P (and indirectly PI(4,5)P_2) control, it also affects PM PS levels because of the ability of these proteins to also transport PS. Indeed, we found that PIP5K overexpression greatly reduced the amount of PS in the PM, which can be the consequence of the much-reduced PI4P gradient between the PM and the ER. One cannot rule out, however, that PIP5K overexpression alters PS levels by alternative ways, such as enhancing endocytosis at the PM. Either way, PI(4,5)P_2 production will affect the PS homeostasis of the cell.

The unique sensory feature of these ORP proteins clearly lies within their N termini. ORP5 and ORP8 both have a PH domain close to the N terminus that was described as binding to PM PI4P and even suggested as a useful tool to specifically monitor PI4P changes in the PM (Chung et al., 2015; Chen et al., 2017). However, the strictly defined PH domains of both ORPs showed poor membrane binding that was greatly increased by the inclusion of a polybasic sequence found toward the N termini and adjacent to the PH domain (termed here as ePH; see Fig. 3 B). In each case, PI(4,5)P_2 further increased the membrane binding of the isolated ePH, but the effect was more prominent in the ORP8 ePH. Binding of PI4P and PI(4,5)P_2 was confirmed in liposome-binding assays using recombinant ePH domain of ORP8. Notably, extension of the ORP8 PH to include the entire N terminus (beyond

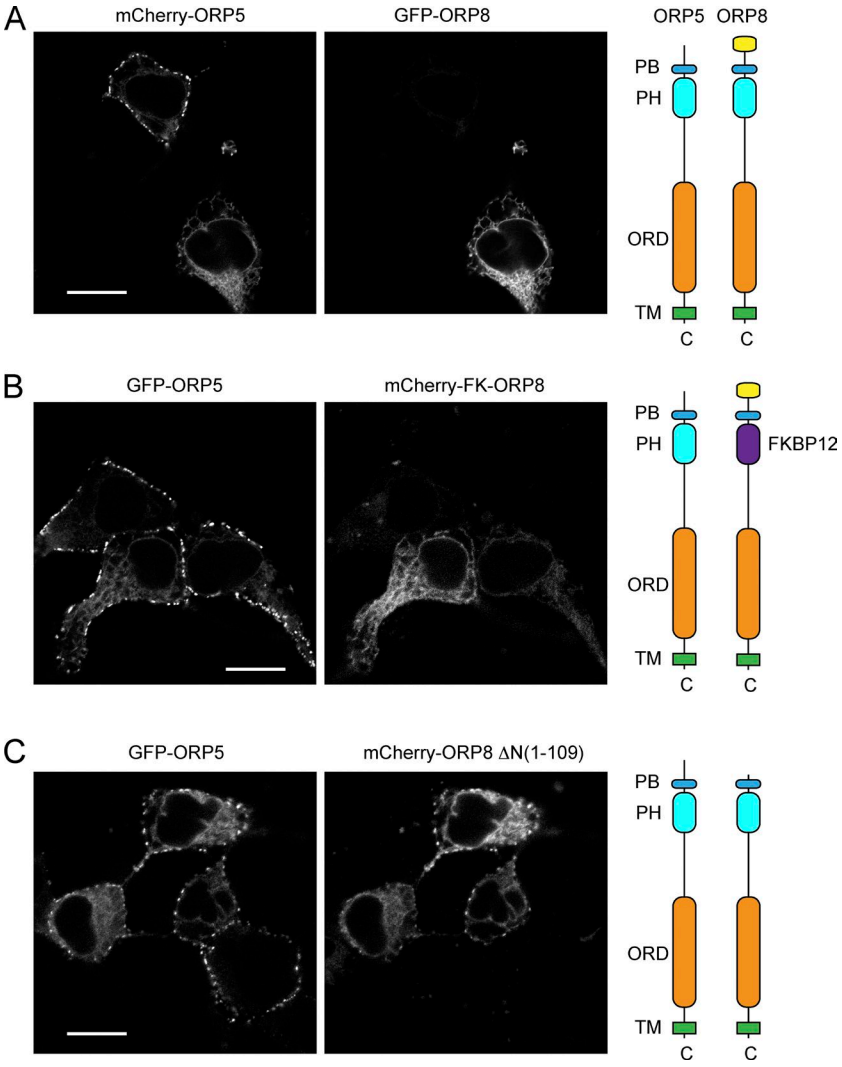

Figure 7. **Molecular interaction between ORP5 and ORP8 affects their PM localization. (A)** Representative live-cell confocal images of cells expressing full-length ORP5 and ORP8 (left) and the cartoon of their structural features (right). Abbreviations are the same as used in Fig. 1, and the yellow box designates the acidic N-terminal stretch present in ORP8 but not ORP5. HEK293-AT1 cells were cotransfected with mCherry-tagged ORP5 and GFP-tagged ORP8 for 1 d for confocal analysis. Note the lack of punctate ORP5 signal in the ORP8-expressing cell. **(B)** Representative images showing cells coexpressing GFP-ORP5 and mCherry-tagged ORP8 in which the PH domain was replaced by an FKPB12 module (mCherry-FK-ORP8, purple box). mCherry-FK-ORP8 expressing cells show more ORP5 showing up in the ER, but still preserve some PM puncta. **(C)** Representative images showing cells coexpressing full-length GFP-ORP5 and mCherry-tagged ORP8 N-terminally truncated to the same point defined as the start of ePH as described in Fig. 3. Note that the truncated ORP8 is less effective in preventing ORP5 PM localization and shows punctate localization itself. Bars, 10 µm.

the polybasic sequence) had a negative effect on both liposome binding and PM localization. This effect has also been noted by Chung et al. (2015) and was attributed to the acidic residues that are found within the very N-terminal part of the sequence. Our results extended these observations and showed that ORP8 is able to inhibit the membrane attachment of ORP5 requiring its N-terminal sequences. This could explain why overexpression of ORP8 increased the resting level of PI4P, an observation that was contrary to expectations.

NMR spectroscopy has revealed the atomistic details of PIP recognition by the ePH and explains the different affinities for both PI4P and PI(4,5)P_2. All of the hydrogen bonds, with the exception of Ser^{205}, are formed between lysine or arginine residues of the ePH and the PIP groups (Fig. 4 E). The apparent requirement for both PI4P and PI(4,5)P_2 in cellular membranes for ORP5/8 recruitment suggests a cooperative mode for PI4P and PI(4,5)P_2 recognition. However, cooperation is not supported by the in vitro binding data or the shared PIP binding site within the PH domain revealed by our structural analysis. It should be noted that the NMR data we obtained did not allow us to properly characterize the polybasic stretch that precedes the PH domain. This part of the protein was affected by conformational heterogeneity that prevented its actual structural analysis, but based on our cellular studies, this region is still expected to contribute to the coordination and binding of the two PIPs, in agreement with the conclusions of Ghai et al. (2017). Still, a mechanism where the ORP8 ePH senses the total level of PI4P + PI(4,5)P_2 within the PM is consistent with all of the in vitro binding data. We suggest that when the total concentration of PM PI4P + PI(4,5)P_2 exceeds an intrinsic threshold, ORP8 is recruited to help ORP5. In contrast, when the levels of either PI4P or PI(4,5)P_2 decrease, both ORP5 and ORP8 stop functioning efficiently.

A recent study showed control of ORP5/8 proteins by PI(4,5)P_2 (Ghai et al., 2017). Although our data are in agreement with the PI(4,5)P_2 regulation of these proteins, several conclusions of that paper contrast with our findings and conclusions. Ghai et al. (2017) claimed that PM localization of the ORP5/8 proteins is not controlled by PI4P and is solely regulated by PI(4,5)P_2, and that their PH domains only bind PI(4,5)P_2 but not PI4P. Our studies clearly show that PI4P is necessary even when PI(4,5)P_2 levels are maintained or even increased. Moreover, those authors claimed that ORP8 lipid transfer domain is promiscuous and can transfer PI(4,5)P_2, cholesterol, and perhaps other lipids using liposome lipid transfer experiments. The overall conclusion of that paper is

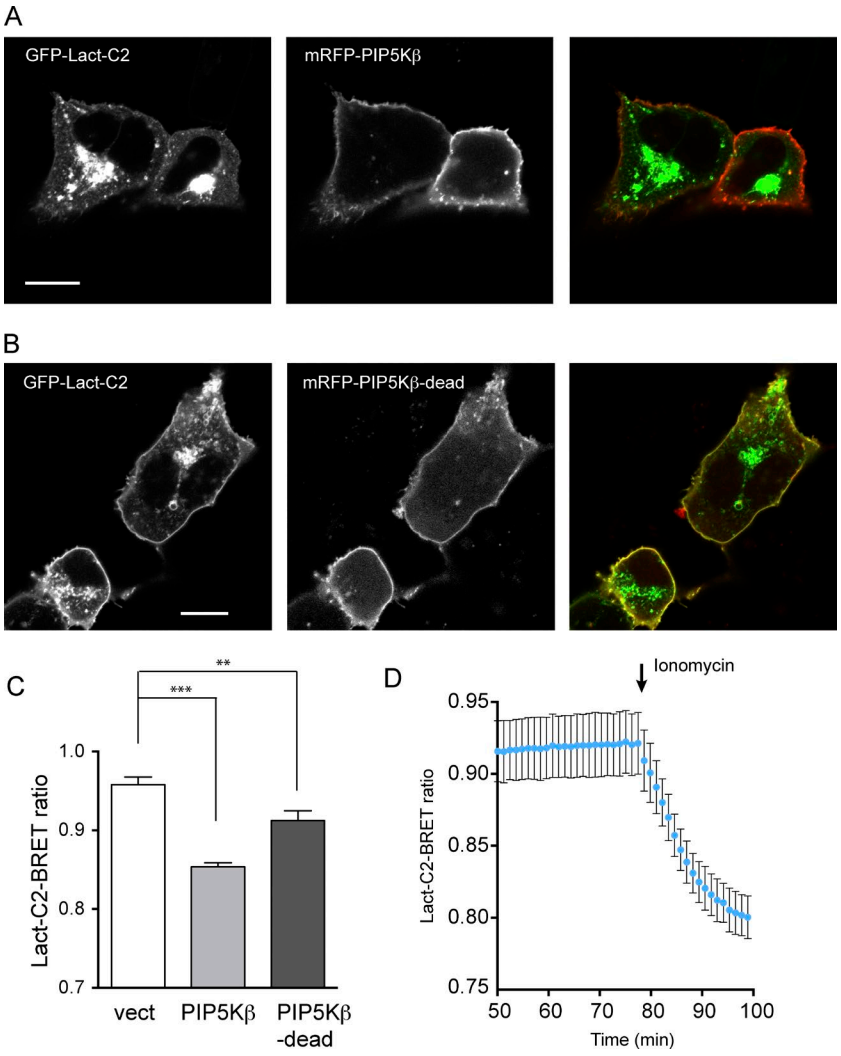

Figure 8. **PIP5Kβ-expressing cells show reduced PM PS levels. (A)** Representative live-cell image displaying PS distribution under overexpression of wild-type PIP5Kβ. HEK293-AT1 cells were cotransfected with GFP-tagged Lact-C2 and mRFP-tagged PIP5Kβ and subjected to confocal microscopy 1 d after transfection. **(B)** Representative live-cell image displaying PS distribution under overexpression of kinase-dead PIP5Kβ. HEK293-AT1 cells were cotransfected with GFP-tagged Lact-C2 and mRFP-tagged PIP5Kβ-dead and subjected to confocal microscopy 1 d after transfection. Bars, 10 µm. **(C)** Quantitation of PM PS levels in wild-type or kinase-dead PIP5Kβ-expressing cells with BRET analysis. HEK293-AT1 cells were transfected with pcDNA3.1(HA) vector, myc-PIP5Kβ, or myc-PIP5Kβ-dead before BRET experiment. PM PS levels were analyzed by measuring mean emission intensity of PM-anchored Venus per Lact-C2-fused luciferase in the presence of coelenterazine h for 7 min. Grand means ± SEM are shown from three independent experiments performed in triplicate. Statistical significance was obtained with two-way ANOVA (***, $P < 0.001$; **, $P < 0.005$). **(D)** Dynamic range of PM PS levels quantitated with BRET. HEK293-AT1 cells were transfected with mCherry empty vector, and PM PS levels were analyzed by measuring mean intensity of PM-anchored Venus per Lact-C2-fused luciferase. After monitoring steady state under DMSO treatment, Ionomycin (10 µM) was treated to deplete PS in the inner leaflet of the PM resulting from PS externalization. Grand means ± SEM are shown from three independent experiments performed in triplicate.

that $PI(4,5)P_2$ rather than PI4P is the driver of PS transport in the cells, contrary to what has been reported and proposed by Chung et al. (2015). Our results show that PI4P is a major cargo of these proteins and its ER transport is an important means by which ORP5/8 proteins control $PI(4,5)P_2$ levels. Our results, based on quantitative BRET measurements and in situ lipid transfer measurements, confirm the primary role of these proteins as PI4P and PS transfer devices. Our studies do not support the role of these proteins as $PI(4,5)P_2$ or cholesterol transport, but rather identify $PI(4,5)P_2$ regulation as primarily serving the need for controlling $PI(4,5)P_2$ levels via regulation of PI4P supply.

In summary, these studies uncover a regulatory role for PM $PI(4,5)P_2$ in the control of ORP5 and ORP8 functions. Through this control, the flux of PI4P from the PM and into the ER is regulated according to the PM PI4P and $PI(4,5)P_2$ status of the cell. Because of the role of the ORP5 and ORP8 proteins in the nonvesicular transport of PS between the ER and the PM, $PI(4,5)P_2$ is also an important indirect regulator of PS metabolism. These observations reveal a new paradigm linking PI4P, $PI(4,5)P_2$, and PS metabolism together, while also facilitating the tight cellular control of $PI(4,5)P_2$ levels within the PM.

Materials and methods

Reagents

Coelenterazine h (1-361301-200) was purchased from Regis Technologies and dissolved in 100% ethanol (vol/vol). PI4KA inhibitor A1 was characterized previously (Bojjireddy et al., 2014). human AngII (05-23-0101), rapamycin (553210), and Ionomycin (407952) were purchased from EMD Millipore. All lipids were purchased from Avanti. Methyl β-cyclodextrin (C4555) was purchased from Sigma-Aldrich. For siRNA experiments, On-TargetPlus Human OSBPL5 (114879) siRNA–SMARTpool (L-009274-01) and On-TargetPlus Human OSBPL8 (114882) siRNA–SMARTpool (L-009508-00) were purchased from Dharmacon. For control siRNA, AllStars Negative Control siRNA (SI03650318) was purchased from Qiagen. Polyclonal anti-OSBPL5 antibody (ab59016) and polyclonal anti-ORP8 antibody (ab84178) were purchased from Abcam; monoclonal anti–α-tubulin was purchased from Sigma-Aldrich (T4026) for Western blot analysis. IRDYE 800CW donkey anti–mouse IgG (H + L; 936-32212), 800CW anti–rabbit IgG (H + L; 926-32211), and 680LT donkey anti–goat IgG (H + L; 926-68024) were purchased from LI-COR and used as secondary antibodies.

DNA constructs

GFP-ORP5 and GFP-ORP8 were cloned as described previously (Sohn et al., 2016). mCherry-ORP5 (ORP5 GenBank accession number: NM_020896) and mCherry-ORP8 (ORP8 GenBank accession number: BC111728) were generated from their respective GFP-tagged versions by replacing GFP to mCherry from pmCherry-C1 vector using NheI–XhoI restriction endonucleases. mRFP-FKBP-INPP5E, PM2-FRB-CFP, and the mRFP-FKBP–fused PJ enzymes have been described previously (Varnai et al., 2006; Hammond et al., 2012). Mouse myc-PIP5Kβ (GenBank accession number: AF048695; human nomenclature) was provided by H. Yin (University of Texas Southwestern Medical Center, Dallas, TX; Rozelle et al., 2000) and CFP-FKBP-PIP5Kγ (GenBank accession number: NM_008844) and CFP-FKBP-PIP5Kγ-dead were provided by T. Meyer (Stanford University, Stanford, CA; Suh et al., 2006). Lyn-targeted nonfluorescent FRB (named PM2-FRB in this study) was from the Meyer laboratory (Inoue et al., 2005). L10-mVenus-T2A-PLCδ1-PH-sLuc and L10-mVenus-T2A-sLuc-P4M(2x) were from the P. Várnai laboratory (Semmelweis University, Budapest, Hungary; Tóth et al., 2016). L10-mVenus-T2A-sLuc-Lact-C2, which is used to measure PS in PM, has been described previously (Sohn et al., 2016). The cholesterol BRET probe was created by cloning the D4H cholesterol-binding domain of perfringolysin O (Maekawa and Fairn, 2015) in place of the P4M(2x) in the L10-mVenus-T2A-sLuc-P4M(2x) construct using XhoI–EcoRI restriction sites. GFP-P4M(2x) was described previously (Hammond et al., 2014). GFP-Lact-C2 was provided by the S. Grinstein laboratory (Hospital for Sick Children, Toronto, Ontario, Canada; Yeung et al., 2008). CFP(W66A)-FKBP-PIP5Kγ and CFP-(W66A)-FKBP-PIP5Kγ-dead were generated with site-directed mutagenesis to inactivate CFP fluorescence to prevent interference with the BRET assay. GFP-ORP8-PLCδ1-PH was cloned by amplifying the PH domain from PLCδ1-PH-GFP (Várnai and Balla, 1998) and inserting it into GFP-ORP8 in place of its PH domain. The PLCδ1-PH PCR product was digested with SalI and SacI restriction endonucleases and ligated with the similarly digested ORP8-derived PCR product that contained the entire GFP-ORP8 plasmid without the ORP8 PH domain. mCherry-ORP5 and mCherry-ORP8 were obtained by replacing GFP with mCherry from the pmCherry-C1 plasmid using NheI–XhoI cuts for ORP5 and AgeI–BsrGI for ORP8. mCherry-ORP8-PLCδ1-PH was generated with the same strategy. GFP-ORP5-ePH was generated by amplifying ePH with PCR from GFP-ORP5 and inserting into pEGFP-C1 vector using EcoRI–KpnI restriction endonucleases. GFP-ORP8-ePH was cloned with PCR amplification of ePH from GFP-ORP8 and with insertion into pEGFP-C1 vector using EcoRI–KpnI restriction enzymes. GFP-ORP5-PH and GFP-ORP8-PH were cloned with the same strategies as GFP-ORP5-ePH and GFP-ORP8-ePH, respectively. For generation of mCherry-FKBP-ORP8, the FKBP12 module was PCR-amplified from mRFP-FK-INPP5E as template (for primers, see Table S1) and inserted into the backbone of GFP-ORP8-PLCδ1-PH, from which the PLCδ1PH domain was removed by Sal1–Sac1 digestion. mCherry-FKBP-ORP5 was generated using the same strategy except that PvuI–HindIII restriction enzymes were used to cut out the PLCδ1PH domain. mCherry-ORP8 ΔN (1–109) was generated by amplifying ORP8, which was N-terminally truncated (coding 1–109 aa residues). The PCR product was inserted by replacing full-length ORP8 in pmCherry-C3 vector just described with BsrGI–XmaI restriction endonucleases. mRFP-PIP5Kβ was cloned by amplifying PIP5Kβ from myc-PIP5Kβ and inserting it into the pmRFP-C1 vector using BglII–KpnI restriction enzymes. Because of an internal KpnI site, the inserted PIP5Kβ was truncated at residue 464 but it was still catalytically active. Generation of myc-PIP5Kβ-dead and mRFP-PIP5Kβ-dead was designed by mutating D203 to A (D203A) with site-directed mutagenesis. D203A in PIP5Kβ corresponds to D253A in PIP5Kγ. Primers used in cloning procedures are listed in Table S1.

Cell culture and transfection

The HEK293-AT1 cell line that stably expresses the rat AT1a angiotensin receptor has been described previously (Balla et al., 2008). This cell line has been regularly tested for *Mycoplasma* contamination and, when thawed, treated with Plasmocin prophylactic (InvivoGen) at 500 µg/ml for 1 wk. HEK293-AT1 cells were cultured in DMEM (high glucose) containing 10% (vol/vol) FBS, penicillin/streptomycin, and 5 µg/ml Plasmocin prophylactic. COS-7 cells (also tested for *Mycoplasma*) were cultivated in DMEM containing 10% FBS, 100 µg/ml penicillin, 100 µg/ml streptomycin, and 0.1% chemically defined lipid supplement (Thermo Fisher Scientific). For confocal microscopy, HEK-AT1 cells (500,000 cells/dish in 2 ml) were seeded onto glass-bottom dishes (30-mm diameter) precoated with poly-L-lysine (PLL), transfected, and subjected to confocal microscopy. For TIRF microscopy, COS-7 cells were seeded in 2-ml volume on 0.1 mg/ml fibronectin–coated glass-bottom 35-mm dishes (CellVis), transfected, and subjected to TIRF microscopy. For BRET measurements, HEK-AT1 cells (30,000 cells/well, in triplicate) were plated onto white 96-well plates that were precoated with PLL, transfected, and subjected to BRET analysis. HEK-AT1 cells were transfected with Effectene transfection reagent (Qiagen), and COS-7 cells were transfected with Lipofectamine 2000 reagent (Thermo Fisher Scientific). For confocal microscopy, cells were transfected with DNA (0.2 µg DNA each) by using Effectene transfection reagent based on the manufacturer's standard protocol. For TIRF microscopy, cells were transfected with 1 µg total DNA precomplexed to 3 µg Lipofectamine 2000 in 200 µl Opti-MEM. The cells were incubated for 1 d after transfection before confocal or TIRF microscopy. For BRET measurements, cells were transfected with DNA (0.1 µg per DNA each). For the recruitment of FKBP-fusion protein to PM, PM2-FRB was cotransfected with the indicated iRFP-tagged FKBP-fused enzyme (0.1 µg per DNA each). Transfected cells were incubated for 1 d, and BRET measurement was performed as described in BRET analysis. Because of high toxicity, mRFP-PIP5Kβ, myc-PIP5Kβ, and CFP(W66A)-FKBP-PIP5Kγ were transfected with very low DNA concentrations (0.5–16 ng/well). For confocal microscopy using both siRNA and DNA transfection, 300,000 cells/dish of HEK-AT1 were seeded and transfected with the indicated siRNA (100 nM for single knockdown and 75 nM each for double knockdown) using 8 µl/dish of Lipofectamine RNAiMAX Transfection Reagent (Thermo Fisher Scientific) 1 d after cell seeding. 0.2 µg GFP-P4M(2x) or GFP-Lact-C2 and 50 ng mRFP-PIP5Kβ were cotransfected 1 d after siRNA transfection with Effectene transfection reagent. 1 d after DNA transfection,

cells were subjected to confocal microscopy. For BRET analysis using both siRNA and DNA transfection, 20,000 cells/well (in triplicate) of HEK-AT1 cells were seeded and transfected with total 150 nM siRNA/well (150 nM siControl or 75 nM siORP5 plus 75 nM siORP8) using 1.2 µl/well Lipofectamine RNAiMAX Transfection Reagent 1 d after cell seeding. 1 d after siRNA transfection, cells were transfected with DNA as just described. For Western blot analysis, HEK-AT1 cells (300,000 cells/well) were seeded onto a PLL-coated 12-well dish and transfected with 100 nM of the indicated siRNA using 2 µl/well Lipofectamine RNAiMAX Transfection Reagent after 1 d of cell seeding.

Live-cell confocal imaging

Transfected cells were incubated in 1 ml modified Krebs-Ringer buffer (120 mM NaCl, 4.7 mM KCl, 1.2 mM $CaCl_2$, 0.7 mM $MgSO_4$, 10 mM glucose, and 10 mM Na-Hepes, pH 7.4). Confocal microscopy was performed at room temperature with a Zeiss laser confocal microscope (LSM 510, 710, or 780) with Zen software. A 1.4-NA, 63× oil-immersion objective was used for all confocal analysis.

TIRF microscopy

cells were imaged at room temperature in FluroBrite medium supplemented with 10% (vol/vol) FBS and 0.1% chemically defined lipid supplement, 2 mM glutamax (Thermo Fisher Scientific), and 25 mM Na-Hepes, pH 7.4. Imaging was performed on a Nikon Eclipse TiE inverted microscopy stand with a Nikon TIRF illuminator with a fiber-coupled LUN-V four-line laser launch (Nikon), Lambda 10-2 emission wheel (Sutter), and Zyla 5.5 sCMOS camera (Andor). GFP and iRFP fluorescence were imaged with 488- and 642-nm excitation, respectively, with a dual-emission filter collecting 505–550 and 650–850 nm (Chroma). mCherry was excited with 561-nm excitation and a dual-emission filter collecting 420–480 and 570–620 nm (Chroma). A 1.45-NA 100× plan-apochromatic oil-immersion objective (Nikon) was used. Cells were stimulated by bath application of 1 µM rapamycin during image acquisition as indicated.

Protein expression and purification

Sequences encoding ORP8 1–271 and ORP8 91–271 were cloned into a homemade vector pHis2 with a T7 promoter and an N-terminal 6× His-tag followed by TEV protease cleavage site. Both labeled and unlabeled proteins were expressed and purified using our standard protocols (Klima et al., 2016). In brief, the constructs were transferred into *Escherichia coli* BL21 (DE3) Star cells (Invitrogen). Transformed cells were grown in autoinduction medium at 37°C until they reached OD_{600} 0.6, then the culture was cultivated at 18°C for an additional 16–18 h. Cells were harvested by centrifugation at 5000 *g* for 10 min at 4°C and lysed using EmulsiFlex-C3 homogenizer (Avestin). Proteins were first purified by affinity chromatography using Ni-NTA resin (Macherey-Nagel), and the His-tag was cleaved off by TEV protease. The proteins were further purified by size exclusion chromatography on a HiLoad 16/10 Sepharose High Performance 75 column (GE Healthcare) in 10 mM Tris, pH 8.0, 200 mM NaCl, and 3 mM β-mercaptoethanol. For NMR experiments, ORP8 (residues 91–271) was expressed as ^{15}N- or $^{15}N/^{13}C$-labeled protein in cells grown in minimal medium containing 0.8 g/liter [^{15}N]ammonium chloride and 2 g/liter D-[^{13}C] glucose. Expression was induced with 0.4 mM IPTG at OD_{600} 0.6; the purification procedure was the same as just described, except size exclusion chromatography was performed in PBS buffer supplemented with 0.5 mM TCEP and 0.01% NaN_3.

Förster resonance energy transfer–based liposome binding assay

Large unilamellar vesicles (LUVs) were used for the binding studies. The lipid mixture containing 2.5 µmol total lipid was placed in a glass test tube and dried by a flow of nitrogen. The lipid film was incubated in vacuum overnight to remove traces of the organic solvents. The film was rehydrated with 0.5 ml LUV buffer (10 mM Tris, pH 7.4, 150 mM NaCl, 20 mM imidazole, and 3 mM β-mercaptoethanol), and the multilamellar vesicles were extruded 20 times with the use of 100-nm filters in the extruder (Avanti Polar Lipids). The LUV lipid mixture consisted of 5 mol % of the following: PI4P, $PI(4,5)P_2$, PI4P/$PI(4,5)P_2$ (1:1 molar ratio), and no phosphoinositides for control (25 – mol % [PI4P] – 2× mol % [$PI(4,5)P_2$]) POPS, 20 mol % cholesterol, 10 mol % 18:1 dansyl PE, and POPC. The binding of the PH domains to the liposomes of defined lipid composition was measured by Förster resonance energy transfer from the tryptophan residues of the protein to the dansyl-labeled liposomes. For that, 300 µl of buffer was mixed with 100 µl of LUVs and titrated with the protein (100 nM to 1.5 µM final). At each protein addition, the fluorescence spectrum was acquired on a Fluoromax-4 fluorescence spectrometer (Horiba). Tryptophan was excited at 291 nm, and the dansyl fluorescence spectrum was measured at 300–570 nm. Each spectrum in the presence of the protein was corrected by subtraction of the spectrum of the LUV solution without added protein to remove the background. The fluorescence intensity at its maximum (522 nm) was plotted as a function of the protein concentration.

NMR spectroscopy

The sample volume was 0.35 ml, with 200- and 50-µM concentrations of the $^{13}C/^{15}N$ and ^{15}N-labeled protein in the NMR buffer (25 mM sodium phosphate, pH 6.5, 100 mM NaCl, 1 mM TCEP, and 0.01% NaN_3), 10% D_2O/90% H_2O. A series of double- and triple-resonance spectra (Renshaw et al., 2004; Veverka et al., 2006) were recorded to determine sequence-specific resonance backbone assignments. The binding of PI4P and $PI(4,5)P_2$ was evaluated by following the specific changes of the backbone amide signals in the 2D $^{15}N/^{1}H$ SOFAST HSQC spectra (Schanda and Brutscher, 2005) of the ^{15}N-labeled protein. 5 mM stock solutions of either PI4P or $PI(4,5)P_2$ were added to protein samples to obtain final ligand concentrations of 0, 25, 50, 100, and 200 µM. SOFAST spectra were acquired with a free induction decay resolution of 20 Hz in both domains, and typical experimental time was 10 min (initial concentration) to 40 min (final concentration). The ligand docking on the PH domain structure driven by NMR data and followed by the 1-ns molecular dynamics calculation in explicit water was performed using Yasara (http://www.yasara.org; Krieger and Vriend, 2014).

BRET analysis

After 24 h of transfection, HEK-AT1 cells were rinsed with modified Krebs-Ringer buffer. Cells were incubated in 50 µl/well

Krebs-Ringer buffer for 30 min before measurement. The entire procedure was conducted at room temperature from preincubation to measurement. For the BRET measurement using A1, cells were subjected to baseline measurement for 4 min (1 min/cycle) with luciferase substrate coelenterazine h in additional 40 µl/well Krebs-Ringer buffer. 10 µl/well Krebs-Ringer buffer containing DMSO or A1 (final concentration 30 nM) was added to the cells, and BRET measurement was conducted for an additional time as indicated (1 min/cycle). For the experiment with FKBP-fused proteins, baseline measurement was conducted for 4 min (15 s/cycle) with coelenterazine h before rapamycin treatment. 10 µl/well Krebs-Ringer buffer containing DMSO or rapamycin (final concentration 100 nM) was added to the cells, and BRET measurement was conducted for the indicated time (15 s/cycle). When there was posttreatment with A1, the measurement was conducted initially with rapamycin for 20 min and then with A1 mixed in 10 µl Krebs-Ringer buffer for 30 min (15 s/cycle). When there was pretreatment with A1, the measurement was conducted initially with A1 for 10 min and then with rapamycin mixed in 10 µl Krebs-Ringer buffer for 30 min (15 s/cycle). For the experiment using AngII stimulation (final concentration 100 nM), cells were subjected to baseline measurement with coelenterazine h for 4 min (15 s/cycle) as just described and stimulated with AngII added in 10 µl Krebs-Ringer buffer. BRET measurement after AngII was conducted for 30 min (15 s/cycle). For showing dynamic range of PM PS levels, vector (pmCherry-C1)-transfected cells were subjected to BRET measurement with the same protocol as A1-treated samples except that DMSO was added instead of A1. Ionomycin (10 µM final concentration) diluted in 10 µl Krebs-Ringer buffer was added at the end of the measurement, and PS decline driven by externalization was monitored for an additional 20 min. For cholesterol extraction experiments, methyl-β-cyclodextrin was diluted in 10 µl Krebs-Ringer buffer and added after baseline BRET measurements (2 mM final). For BRET analysis of resting PM PI4P and PI(4,5)P_2 levels, BRET values were calculated from measurements performed for 4–7 min after adding coelenterazine h. A Tristar2 LB 942 Multimode Microplate Reader (Berthold Technologies) equipped with 540/40-nm (Venus fluorescent measurement) and 475/20-nm (Luciferase measurement) emission filters were used for BRET.

SDS-PAGE and Western blot analysis

2 d after transfection, cells were lysed with 200 µl/well of 1× Laemmli buffer, and lysates were gently denatured at 65°C for 30 min in Eppendorf tubes before SDS-PAGE. 40 µl of each sample was loaded onto 4–12% Tris-glycine mini-gel (Thermo Fisher Scientific). After SDS-PAGE at 110 V in Tris-glycine SDS running buffer (Thermo Fisher Scientific), proteins were transferred to nitrocellulose membranes (0.45 µm pore size; Thermo Fisher Scientific) at 100 V for 1 h in Tris-glycine transfer buffer (Thermo Fisher Scientific) containing 5% methanol (vol/vol). Nonspecific antibody binding was blocked with Odyssey Blocking Buffer (LI-COR) for 1 h at room temperature. Primary antibodies were diluted in 5% BSA-PBS solution (wt/vol) and incubated at 4°C overnight. Primary antibodies were diluted in the following ratio: α-tubulin 1:2,000, α-OSBPL5 1:500, and α-ORP8 1:500. After three washes (for 10 min each) with 0.1% Tween 20–containing PBS solution (vol/vol), fluorescence-conjugated secondary antibodies (diluted 1:5,000) were incubated in PBS-containing 5% BSA at room temperature for 1 h. Fluorescence signal was detected with the Odyssey 9120 imaging system (LI-COR), and the images obtained from individual wavelengths were presented with grayscale by using OdysseyV3.0 software.

Data processing, calculations, and statistics

PM PI4P, PI(4,5)P_2, and PS levels in resting cells measured by BRET analysis are presented as grand means ± SEM from three independent experiments performed in triplicate. BRET values in each experiment were normalized to the mean value of the control group. The representative BRET result showing dose-dependent overexpression of myc-PIP5Kβ is shown as means ± SD normalized to the initial BRET value of the group without transfection. The correlation between the rate of PI4P clearance and initial PI4P levels in the PM was analyzed with BRET measurement of dose-dependent overexpression of myc-PIP5Kβ and calculation of the slopes from the highest point of PI4P levels for a 1,000-s time window. Quantitation of the PM interaction of ORP5 was analyzed as the change of fluorescence intensity of ORP5 in TIRF microscopy in the evanescent field for 28–34 cells, and grand means ± SEM from three independent experiments are presented. Statistical significance was calculated with one-way ANOVA using GraphPad Prism software. For multiple comparisons, two-way ANOVA was performed with Tukey's multiple comparison test. Confocal pictures and Western blot scans were processed in Adobe Photoshop, and minimal and maximal intensities were adjusted to use the whole dynamic range. No change of linearity (gamma) was allowed.

Online supplemental material

Fig. S1 shows PM engagement of ORP8-PLCδ-PH and principal of BRET analysis. Fig. S2 shows characterization of the abilities of recruitable ORP5/8 proteins to extract PS, PI(4,5)P_2, and cholesterol from the PM. Fig. S3 shows disengagement of ORP5 and ORP5-ePH from the PM in response to PM recruitment of INPP5E phosphatase. Fig. S4 shows NMR spectra changes upon PI4P and PI(4,5)P_2 binding to the ORP8 PH domain. Fig. S5 shows effects of PIP5K on PM PI4P levels and efficiency of knockdown. Table S1 shows the PCR primers used in this study.

Acknowledgments

We are grateful for DNA constructs provided by the Grinstein, Meyer, Yin, and Varnai laboratories. Confocal imaging was performed at the Microscopy and Imaging Core of the National Institute of Child Health and Human Development, National Institutes of Health, with the kind assistance of Dr. Vincent Schram. We also thank Dr. Joshua Pemberton for critical reading of the manuscript.

This work was supported in part by the intramural research program of the Eunice Kennedy Shriver National Institute of Child Health and Human Development at the National Institutes of Health. The work of J.P. Zewe, R.C. Wills, and G.R.V. Hammond was supported by National Institutes of Health grant 1R35GM119412-01 (to G.R.V. Hammond). The work of

J. Humpolickova, L. Vrzal, D. Chalupska, V. Veverka, and E. Boura was supported by a grant from the Czech Science Foundation (17-05200S, to E. Boura) and by the Academy of Sciences of the Czech Republic (RVO:61388963). G.D. Fairn was supported by a Canadian Institutes of Health Research open operating grant (MOP-133656).

The authors declare no competing financial interest.

Author contributions: M. Sohn performed BRET experiments and data analysis; M. Sohn and T. Balla designed research, performed confocal microscopy and data analysis, and wrote the manuscript; M. Sohn, M. Korzeniowski, G.D. Fairn, and T. Balla generated DNA constructs; J.P. Zewe, R.C. Wills, and G.R.V. Hammond performed TIRF experiments and data analysis; and J. Humpolickova, L. Vrzal, D. Chalupska, V. Veverka, and E. Boura generated recombinant proteins and performed the NMR analysis and liposome binding assays, including data analysis.

Submitted: 16 October 2017
Revised: 5 January 2018
Accepted: 30 January 2018

References

Balla, T. 2013. Phosphoinositides: Tiny lipids with giant impact on cell regulation. *Physiol. Rev.* 93:1019–1137. https://doi.org/10.1152/physrev.00028.2012

Balla, A., Y.J. Kim, P. Varnai, Z. Szentpetery, Z. Knight, K.M. Shokat, and T. Balla. 2008. Maintenance of hormone-sensitive phosphoinositide pools in the plasma membrane requires phosphatidylinositol 4-kinase IIIalpha. *Mol. Biol. Cell.* 19:711–721. https://doi.org/10.1091/mbc.E07-07-0713

Baskin, J.M., X. Wu, R. Christiano, M.S. Oh, C.M. Schauder, E. Gazzerro, M. Messa, S. Baldassari, S. Assereto, R. Biancheri, et al. 2016. The leukodystrophy protein FAM126A (hyccin) regulates PtdIns(4)P synthesis at the plasma membrane. *Nat. Cell Biol.* 18:132–138. https://doi.org/10.1038/ncb3271

Bojjireddy, N., J. Botyanszki, G. Hammond, D. Creech, R. Peterson, D.C. Kemp, M. Snead, R. Brown, A. Morrison, S. Wilson, et al. 2014. Pharmacological and genetic targeting of the PI4KA enzyme reveals its important role in maintaining plasma membrane phosphatidylinositol 4-phosphate and phosphatidylinositol 4,5-bisphosphate levels. *J. Biol. Chem.* 289:6120–6132. https://doi.org/10.1074/jbc.M113.531426

Boura, E., and R. Nencka. 2015. Phosphatidylinositol 4-kinases: Function, structure, and inhibition. *Exp. Cell Res.* 337:136–145. https://doi.org/10.1016/j.yexcr.2015.03.028

Chen, Y.J., C.L. Chang, W.R. Lee, and J. Liou. 2017. RASSF4 controls SOCE and ER–PM junctions through regulation of PI(4,5)P_2. *J. Cell Biol.* 216:2011–2025. https://doi.org/10.1083/jcb.201606047

Chung, J., F. Torta, K. Masai, L. Lucast, H. Czapla, L.B. Tanner, P. Narayanaswamy, M.R. Wenk, F. Nakatsu, and P. De Camilli. 2015. PI4P/phosphatidylserine countertransport at ORP5- and ORP8-mediated ER-plasma membrane contacts. *Science.* 349:428–432. https://doi.org/10.1126/science.aab1370

Dickson, E.J., J.B. Jensen, O. Vivas, M. Kruse, A.E. Traynor-Kaplan, and B. Hille. 2016. Dynamic formation of ER-PM junctions presents a lipid phosphatase to regulate phosphoinositides. *J. Cell Biol.* 213:33–48. https://doi.org/10.1083/jcb.201508106

Ghai, R., X. Du, H. Wang, J. Dong, C. Ferguson, A.J. Brown, R.G. Parton, J.W. Wu, and H. Yang. 2017. ORP5 and ORP8 bind phosphatidylinositol-4, 5-biphosphate (PtdIns(4,5)P 2) and regulate its level at the plasma membrane. *Nat. Commun.* 8:757. https://doi.org/10.1038/s41467-017-00861-5

Giordano, F., Y. Saheki, O. Idevall-Hagren, S.F. Colombo, M. Pirruccello, I. Milosevic, E.O. Gracheva, S.N. Bagriantsev, N. Borgese, and P. De Camilli. 2013. PI(4,5)P(2)-dependent and Ca(2+)-regulated ER-PM interactions mediated by the extended synaptotagmins. *Cell.* 153:1494–1509. https://doi.org/10.1016/j.cell.2013.05.026

Hammond, G.R., M.J. Fischer, K.E. Anderson, J. Holdich, A. Koteci, T. Balla, and R.F. Irvine. 2012. PI4P and PI(4,5)P2 are essential but independent lipid determinants of membrane identity. *Science.* 337:727–730. https://doi.org/10.1126/science.1222483

Hammond, G.R., M.P. Machner, and T. Balla. 2014. A novel probe for phosphatidylinositol 4-phosphate reveals multiple pools beyond the Golgi. *J. Cell Biol.* 205:113–126. https://doi.org/10.1083/jcb.201312072

Inoue, T., W.D. Heo, J.S. Grimley, T.J. Wandless, and T. Meyer. 2005. An inducible translocation strategy to rapidly activate and inhibit small GTPase signaling pathways. *Nat. Methods.* 2:415–418. https://doi.org/10.1038/nmeth763

Klima, M., D.J. Tóth, R. Hexnerova, A. Baumlova, D. Chalupska, J. Tykvart, L. Rezabkova, N. Sengupta, P. Man, A. Dubankova, et al. 2016. Structural insights and in vitro reconstitution of membrane targeting and activation of human PI4KB by the ACBD3 protein. *Sci. Rep.* 6:23641. https://doi.org/10.1038/srep23641

Krieger, E., and G. Vriend. 2014. YASARA View—molecular graphics for all devices—from smartphones to workstations. *Bioinformatics.* 30:2981–2982. https://doi.org/10.1093/bioinformatics/btu426

Lacalle, R.A., J.C. de Karam, L. Martínez-Muñoz, I. Artetxe, R.M. Peregil, J. Sot, A.M. Rojas, F.M. Goñi, M. Mellado, and S. Mañes. 2015. Type I phosphatidylinositol 4-phosphate 5-kinase homo- and heterodimerization determines its membrane localization and activity. *FASEB J.* 29:2371–2385. https://doi.org/10.1096/fj.14-264606

Maeda, K., K. Anand, A. Chiapparino, A. Kumar, M. Poletto, M. Kaksonen, and A.C. Gavin. 2013. Interactome map uncovers phosphatidylserine transport by oxysterol-binding proteins. *Nature.* 501:257–261. https://doi.org/10.1038/nature12430

Maekawa, M., and G.D. Fairn. 2015. Complementary probes reveal that phosphatidylserine is required for the proper transbilayer distribution of cholesterol. *J. Cell Sci.* 128:1422–1433. https://doi.org/10.1242/jcs.164715

Moser von Filseck, J., A. Čopič, V. Delfosse, S. Vanni, C.L. Jackson, W. Bourguet, and G. Drin. 2015. Phosphatidylserine transport by ORP/Osh proteins is driven by phosphatidylinositol 4-phosphate. *Science.* 349:432–436. https://doi.org/10.1126/science.aab1346

Nakatsu, F., J.M. Baskin, J. Chung, L.B. Tanner, G. Shui, S.Y. Lee, M. Pirruccello, M. Hao, N.T. Ingolia, M.R. Wenk, and P. De Camilli. 2012. PtdIns4P synthesis by PI4KIIIα at the plasma membrane and its impact on plasma membrane identity. *J. Cell Biol.* 199:1003–1016. https://doi.org/10.1083/jcb.201206095

Olkkonen, V.M., and S. Li. 2013. Oxysterol-binding proteins: Sterol and phosphoinositide sensors coordinating transport, signaling and metabolism. *Prog. Lipid Res.* 52:529–538. https://doi.org/10.1016/j.plipres.2013.06.004

Renshaw, P.S., V. Veverka, G. Kelly, T.A. Frenkiel, R.A. Williamson, S.V. Gordon, R.G. Hewinson, and M.D. Carr. 2004. Sequence-specific assignment and secondary structure determination of the 195-residue complex formed by the Mycobacterium tuberculosis proteins CFP-10 and ESAT-6. *J. Biomol. NMR.* 30:225–226. https://doi.org/10.1023/B:JNMR.0000048852.40853.5c

Rozelle, A.L., L.M. Machesky, M. Yamamoto, M.H. Driessens, R.H. Insall, M.G. Roth, K. Luby-Phelps, G. Marriott, A. Hall, and H.L. Yin. 2000. Phosphatidylinositol 4,5-bisphosphate induces actin-based movement of raft-enriched vesicles through WASP-Arp2/3. *Curr. Biol.* 10:311–320. https://doi.org/10.1016/S0960-9822(00)00384-5

Schanda, P., and B. Brutscher. 2005. Very fast two-dimensional NMR spectroscopy for real-time investigation of dynamic events in proteins on the time scale of seconds. *J. Am. Chem. Soc.* 127:8014–8015. https://doi.org/10.1021/ja051306e

Sohn, M., P. Ivanova, H.A. Brown, D.J. Toth, P. Varnai, Y.J. Kim, and T. Balla. 2016. Lenz-Majewski mutations in PTDSS1 affect phosphatidylinositol 4-phosphate metabolism at ER-PM and ER-Golgi junctions. *Proc. Natl. Acad. Sci. USA.* 113:4314–4319. https://doi.org/10.1073/pnas.1525719113

Stefan, C.J., A.G. Manford, D. Baird, J. Yamada-Hanff, Y. Mao, and S.D. Emr. 2011. Osh proteins regulate phosphoinositide metabolism at ER-plasma membrane contact sites. *Cell.* 144:389–401. https://doi.org/10.1016/j.cell.2010.12.034

Suh, B.C., T. Inoue, T. Meyer, and B. Hille. 2006. Rapid chemically induced changes of PtdIns(4,5)P2 gate KCNQ ion channels. *Science.* 314:1454–1457. https://doi.org/10.1126/science.1131163

Tóth, J.T., G. Gulyás, D.J. Tóth, A. Balla, G.R. Hammond, L. Hunyady, T. Balla, and P. Várnai. 2016. BRET-monitoring of the dynamic changes of inositol lipid pools in living cells reveals a PKC-dependent PtdIns4P increase upon EGF and M3 receptor activation. *Biochim. Biophys. Acta.* 1861:177–187. https://doi.org/10.1016/j.bbalip.2015.12.005

Varnai, P., B. Thyagarajan, T. Rohacs, and T. Balla. 2006. Rapidly inducible changes in phosphatidylinositol 4,5-bisphosphate levels influence multiple regulatory functions of the lipid in intact living cells. *J. Cell Biol.* 175:377–382. https://doi.org/10.1083/jcb.200607116

Várnai, P., and T. Balla. 1998. Visualization of phosphoinositides that bind pleckstrin homology domains: Calcium- and agonist-induced dynamic changes and relationship to myo-[^{3}H]inositol-labeled phosphoinositide pools. *J. Cell Biol.* 143:501–510. https://doi.org/10.1083/jcb.143.2.501

Várnai, P., G. Gulyás, D.J. Tóth, M. Sohn, N. Sengupta, and T. Balla. 2017. Quantifying lipid changes in various membrane compartments using lipid binding protein domains. *Cell Calcium.* 64:72–82. https://doi.org/10.1016/j.ceca.2016.12.008

Veverka, V., G. Lennie, T. Crabbe, I. Bird, R.J. Taylor, and M.D. Carr. 2006. NMR assignment of the mTOR domain responsible for rapamycin binding. *J. Biomol. NMR.* 36(S1, Suppl 1):3. https://doi.org/10.1007/s10858-005-4324-1

Yeung, T., G.E. Gilbert, J. Shi, J. Silvius, A. Kapus, and S. Grinstein. 2008. Membrane phosphatidylserine regulates surface charge and protein localization. *Science.* 319:210–213. https://doi.org/10.1126/science.1152066

Supplemental material

Sohn et al., https://doi.org/10.1083/jcb.201710095

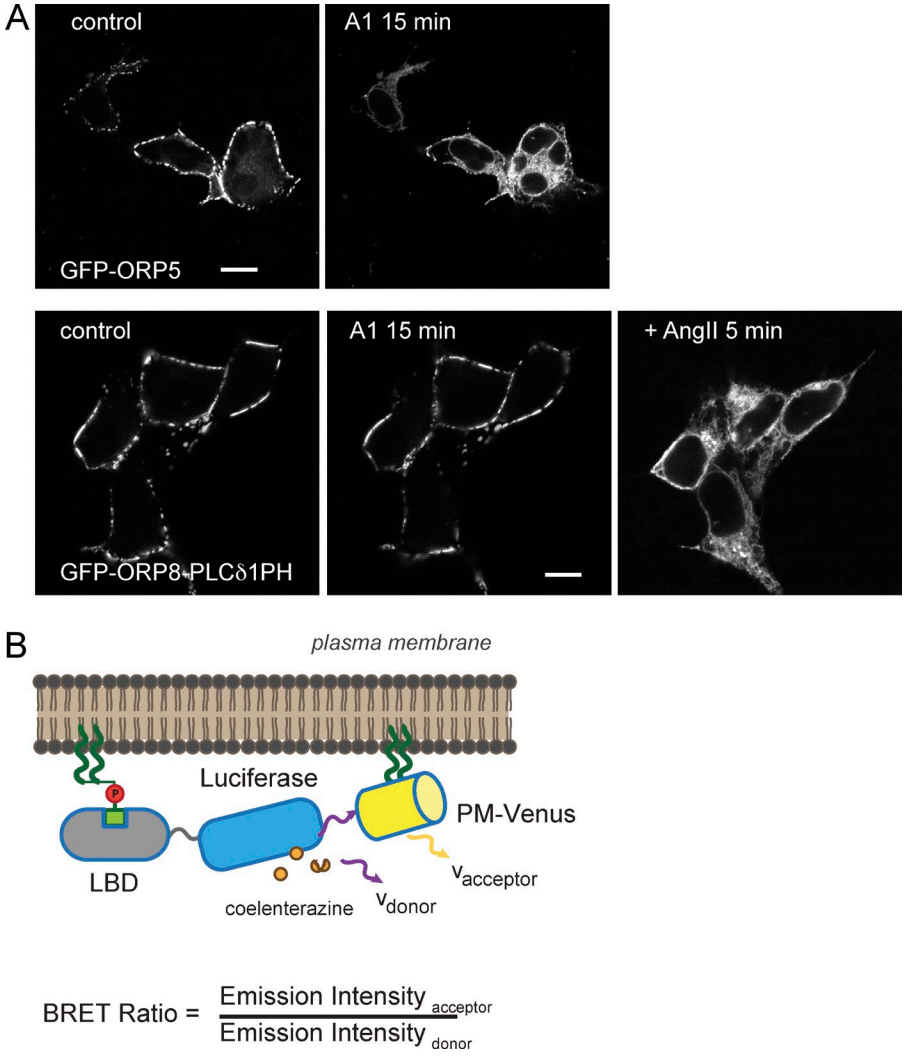

Figure S1. **PM engagement of ORP8-PLCδ-PH and principal of BRET analysis. (A)** Representative live-cell images comparing localization of ORP5 (top) or ORP8-PLCδ1-PH (bottom) in the presence of A1 (100 nM) or A1 plus AngII (100 nM). HEK293-AT1 cells were transfected with GFP-tagged ORP5 or ORP8-PLCδ1-PH and subjected to confocal microscopy after 1 d. Cells were observed with treatment of A1 or A1 plus AngII for the indicated time. Bars, 10 µm. **(B)** Schematic diagram describing the principal of BRET analysis. BRET signal is determined by measuring the proximity between lipid binding domain–fused *s*-luciferase and PM-anchored mVenus. In brief, PM-bound *s*-luciferase (donor) excites PM-anchored mVenus (acceptor) in the presence of coelenterazine h, which is a substrate of luciferase. A change in PM lipid levels increases or decreases PM binding of lipid binding domain–*s*-luciferase and, in turn, the excitation of mVenus. BRET ratio is defined by the emission intensity of mVenus (acceptor) per the emission intensity of *s*-luciferase (donor).

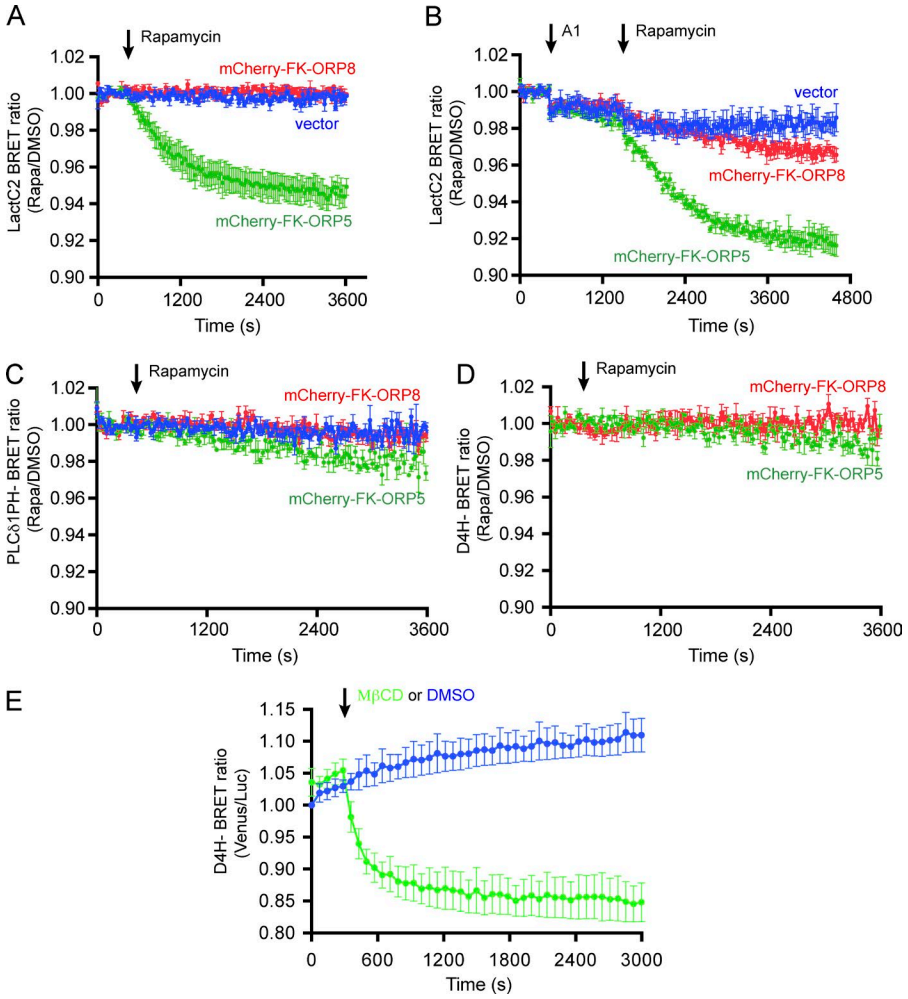

Figure S2. **Characterization of the abilities of recruitable ORP5/8 proteins to extract PS, PI(4,5)P_2, and cholesterol from the PM. (A)** Analysis of PS extraction from PM by PM-recruited ORP5/8. HEK293-AT1 cells were transfected with mCherry or mCherry-tagged FKBP-ORP5 (FK-ORP5) or -ORP8 (FK-ORP8) together with PM-targeted FRB (PM2-FRB). PM PS levels were quantitated with BRET analysis by measuring emission intensity of PM-anchored Venus acquired from Lact-C2–fused luciferase. After baseline measurement, cells were treated with DMSO or rapamycin (100 nM) to recruit FK-ORP5 or -ORP8 to the PM. PS level changes were plotted relative to DMSO-treated controls (rapamycin/DMSO). These ratio values were normalized to those obtained from pretreatment baseline measurement. Grand means ± SEM are shown from three independent experiments performed in triplicate. **(B)** Quantitation of PS extraction from PM by PM-recruited ORP5/8 after treatment with the PI4KA inhibitor, A1 (30 nM), for 10 min. PM PS quantitation was as described in A. Grand means ± SEM are shown from three independent experiments performed in triplicate. **(C)** Quantitation of PI(4,5)P_2 extraction from PM by PM-recruited ORP5/8. HEK293-AT1 cells were transfected and subjected to BRET measurement as described in A except that PM PI(4,5)P_2 levels were quantitated by measuring emission intensity of PM-anchored Venus from PLCδ1-PH–fused luciferase. Grand means ± SEM are shown from three independent experiments performed in triplicate. **(D)** Quantitation of cholesterol extraction from PM by PM-recruited ORP5/8. HEK293-AT1 cells were transfected with mCherry-FK-ORP5 and -ORP8 in addition to PM-anchoring FRB (PM2-FRB). PM cholesterol levels were quantitated by measuring emission intensity of PM-anchored Venus from D4H-fused luciferase. Treatment and measurements were performed as described in A. Grand means ± SEM are shown from three independent experiments performed in triplicate. **(E)** Extraction of cholesterol by treatment with methyl β-cyclodextrin (MβCD; 2 mM) was used to validate the method. Grand means ± SEM are shown from three independent experiments performed in triplicate.

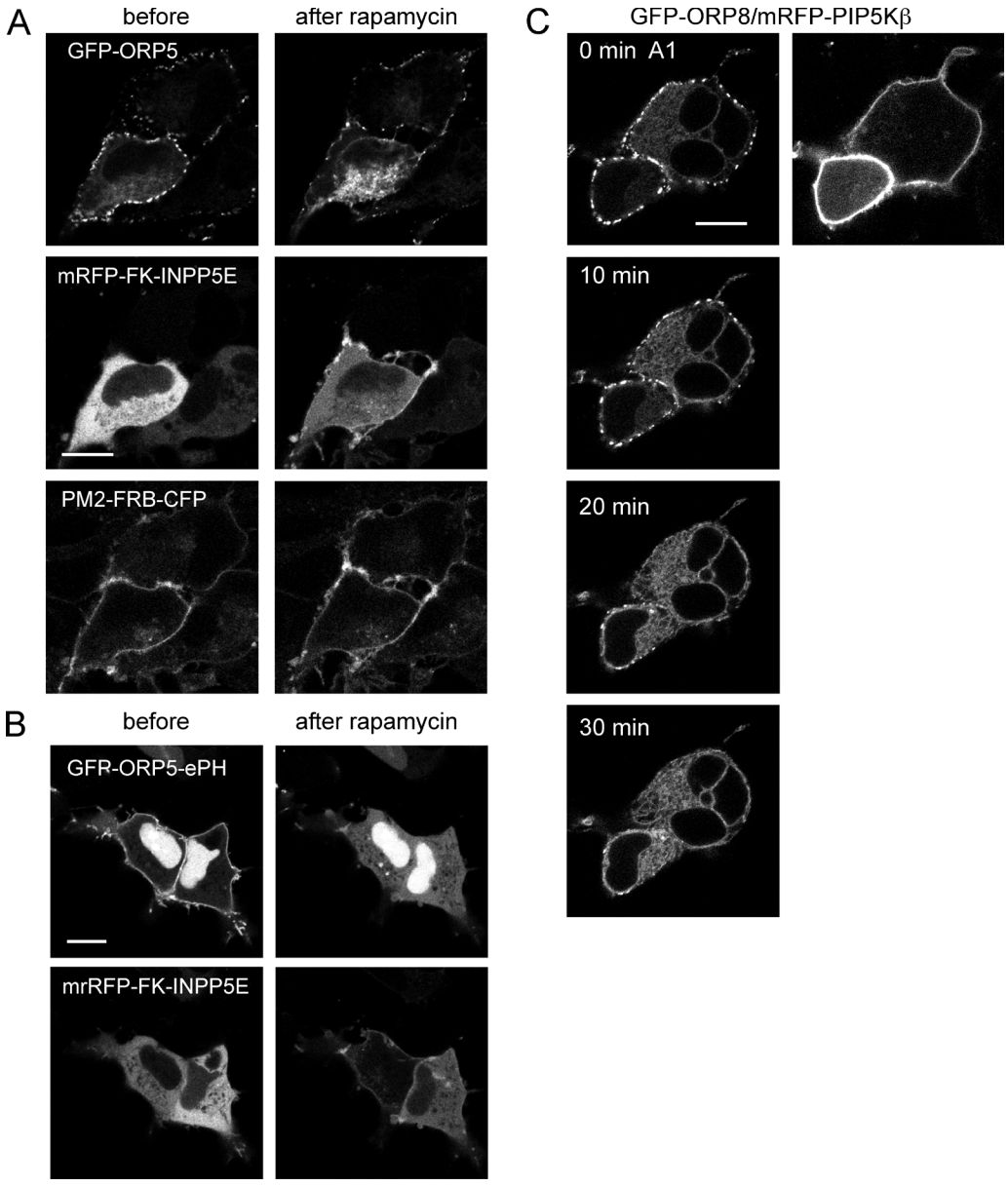

Figure S3. **Disengagement of ORP5 and ORP5-ePH from the PM in response to PM recruitment of INPP5E phosphatase. (A)** Representative live-cell image showing localization of ORP5 before and after recruitment of mRFP-tagged FKBP-INPP5E phosphatase to the PM. HEK293-AT1 cells were transfected with GFP-tagged ORP5, mRFP-tagged FKBP-INPP5E, and CFP-tagged PM2-FRB. After 1 d, cells were subjected to confocal microscopy before (left) and after (right) rapamycin treatment (100 nM, 5 min). **(B)** Representative live-cell image showing localization of ORP5-ePH before and after recruitment of mRFP-tagged FKBP-INPP5E phosphatase to the PM. HEK293-AT1 cells were cells GFP-tagged ORP5-ePH, mRFP-tagged FKBP-INPP5E, and CFP-tagged PM2-FRB. After 1 d, confocal microscopy was performed as described in A. **(C)** Cells were transfected with GFP-ORP8 and mRFP-PIP5Kβ to increase membrane interaction of ORP8. After 1 d of transfection, cells were treated with 100 nM A1, and the localization of GFP-ORP8 was followed by confocal microscopy. Note the slow dissociation of GFP-ORP8 from the PM and appearance in the ER. Bars, 10 µm.

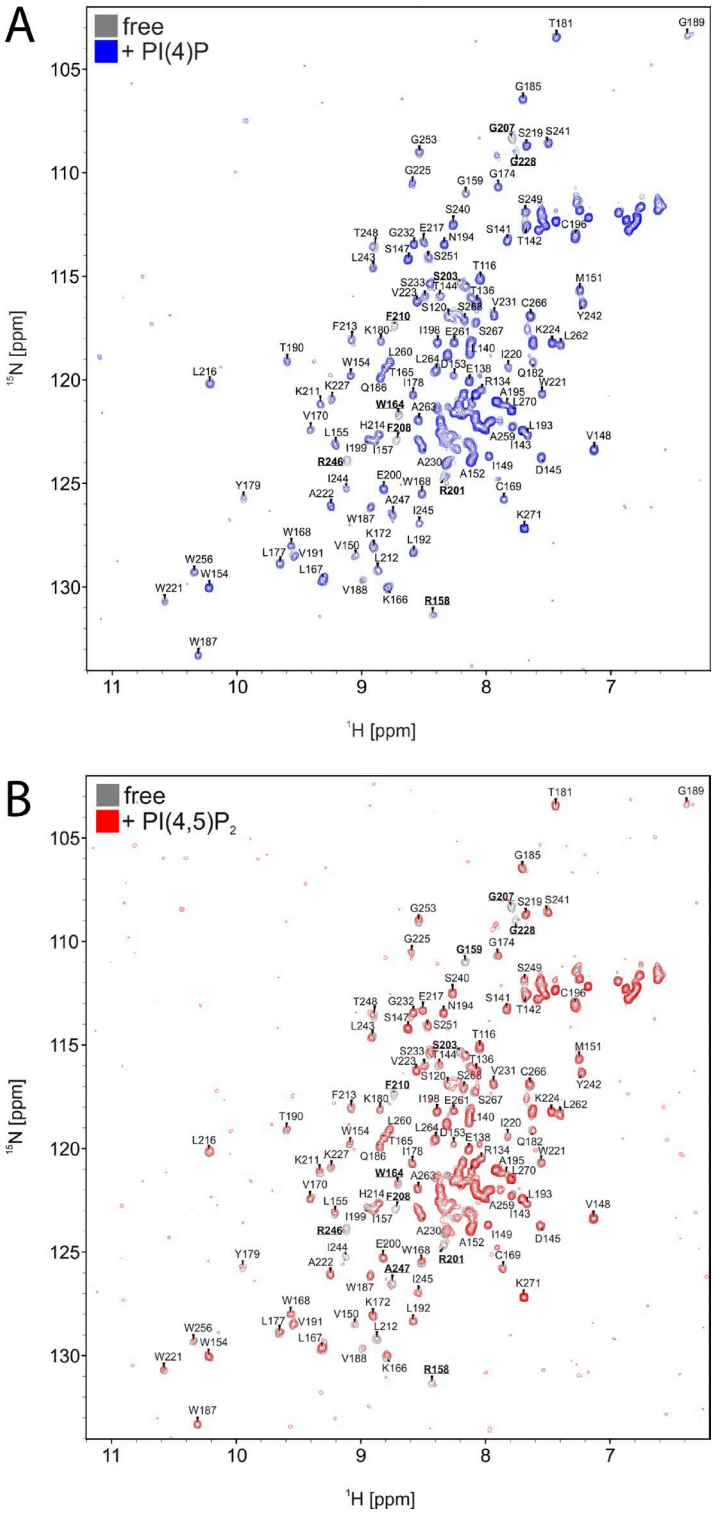

Figure S4. **PI4P and PI(4,5)P_2 binding to the ORP8 PH domain. (A)** Interaction of PI4P-induced specific changes in the 2D $^{15}N/^{1}H$ HSQC NMR spectra of ORP8. The labels of the most affected backbone amide signals of ORP8 are underlined. **(B)** Interaction of PI(4,5)P_2-induced specific changes in the 2D $^{15}N/^{1}H$ HSQC NMR spectra of ORP8. The labels of the most affected backbone amide signals of ORP8 are underlined. This figure includes directly observed NMR spectra for the free and ligand-bound protein in a single experiment.

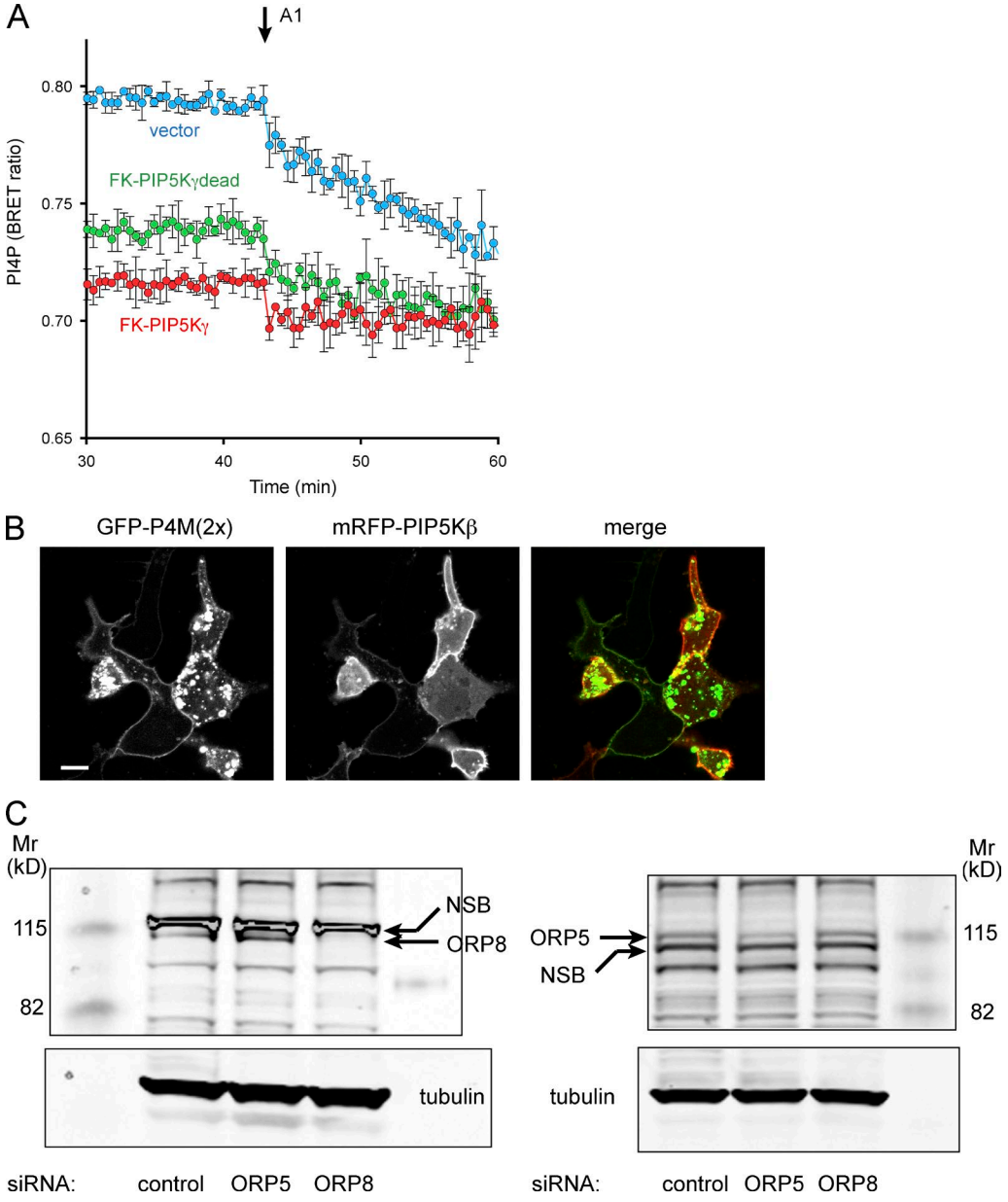

Figure S5. **Effects of PIP5K on PM PI4P levels. (A)** Representative BRET analysis monitoring PI4P clearance from the PM with or without PM-recruited PIP5Kγ. HEK293-AT1 cells were transected with CFP(W66A)-tagged FKBP-PIP5Kγ (wild-type or kinase-dead) and PM2-FRB 1 d before BRET measurement. Control cells were transfected with pcDNA3.1(HA) instead of FKBP-PIP5Kγ. PI4P clearance from the PM was analyzed with BRET by measuring emission intensity of PM-anchored Venus per P4M2x-fused luciferase. After baseline measurement and measurement with rapamycin (100 nM), cells were treated with A1 (30 nM), and PI4P clearance was monitored. Means ± SD are shown from triplicate experiments. **(B)** Representative live-cell image displaying redistribution of PI4P probe by PI5PKβ overexpression. HEK293-AT1 cells were transfected with GFP-tagged P4M2x and mRFP-tagged PIP5Kβ. After 1 d, cells were observed with confocal microscopy. Bar, 10 µm. **(C)** Western blot analysis of cellular extracts after knockdown of ORP5 and ORP8 proteins. NSB, nonspecific bands.

Table S1. **Primers used in this study**

Construct	Template DNA	Primers	Sequence (5′ to 3′)
GFP-ORP8-PLCδ1-PH	pEGFP-C3-ORP8	Forward	ATATGAGCTCAAACGTACAATGATCAGAGAAGGAAAGGAAC
		Reverse	ATATGTCGACACTGAGCAGCTCCTTTGTGGCTC
	pEGFP-N1-PLCδ1-PH	Forward	ATATGTCGACGAGGATCTACAGGCGCTGCTGAAG
		Reverse	ATATGAGCTCGTCCTTGTTTTTGTCAGCTTTTCGC
mRFP-PIP5Kβ	myc-PIP5Kβ	Forward	TATACAAGATCTCGATCGTCTGCTGCTGAAAATGGAGAG
		Reverse	ATATAGGTACCTTATAAATAGACGTCAAGCACAGAAGCATT
mRFP-PIP5Kβ-dead	mRFP-PIP5Kβ	Forward	TTTGACCTATGCCCTGAAAGGCTC
		Reverse	CCTTTCAGGGCATAGGTCAAATGCATC
GFP-ORP5-ePH	pEGFP-C1-ORP5	Forward	TATAGAATTCTTGCAACGGGTCAGACAAGGAATGTGTGTC
		Reverse	TATAGGTACCTACAGTCTCAGTAGGCTAGAGCAGCGCAGG
GFP-ORP8-ePH	pEGFP-C3-ORP8	Forward	TATAGAATTCTAGTTCAACTTCAAGCAAACTCACAAAAAAAGAATCTC
		Reverse	TATAGGTACCTATTTAAGAAGACTAGAACATTTCAAAGCCAACTCCAAAGCATCC
GFP-ORP5-PH	pEGFP-C1-ORP5	Forward	TATAGAATTCTGCTCTGACAGACCCCAGCGTGGTCATC
		Reverse	TATAGGTACCTACAGTCTCAGTAGGCTAGAGCAGCGCAGG
GFP-ORP8-PH	pEGFP-C3-ORP8	Forward	TATAGAATTCTACAATCACAGATCCTTCTGTTATTGTTATGGCTGATTGG
		Reverse	TATAGGTACCTATTTAAGAAGACTAGAACATTTCAAAGCCAACTCCAAAGCATCC
GFP-ORP8 ΔN (1-109)	pEGFP-C3-ORP8	Forward	ATATTGTACAACAGTTCAACTTCAAGCAAACTCAC
		Reverse	ATATCCCGGGTTACTTGAACATGAAGTTTATTATGACTTGAAGC
Cherry-FKBP-ORP5	mRFP-FKBP12-INPP5E	Forward	ATGCAAGCTTACTGGGAGTGCAGGTGGAAACCATC
		Reverse	AATATGCGATCGCAGCTTCCAGTTTTAGAAGCTCCACATCG
	pEGFP-C1-ORP5	Forward	ATAGCGATCGCAACCTGCAAGCCGGGCCGAGAC
		Reverse	ATATAAGCTTGCGCTGAGCAGCTGCCGTGTGGC
mCherry-FKBP-ORP8	mRFP-FKBP12-INPP5E	Forward	ATATGTCGACCTGGGAGTGCAGGTGGAAACCATC
		Reverse	ATATGAGCTCAGCTTCCAGTTTTAGAAGCTCCACATCG
myc-PIP5Kβ-dead	myc-PIP5Kβ	Forward	TTTGACCTATGCCCTGAAAGGCTC
		Reverse	CCTTTCAGGGCATAGGTCAAATGCATC
CFP(W66A)-FKBP-PIP5Kγ, CFP(W66A)-FKBP-PIP5Kγ-dead	CFP-FKBP-PIP5Kγ	Forward	TGCGGTCAGGGTGGTCACGAGGGTG
		Reverse	GGCGTGCAGTGCTTCAGCCGCTAC